# Supporting Information

# Arthpyrones A–C, Pyridone Alkaloids from a Sponge-Derived Fungus *Arthrinium arundinis* ZSDS1-F3

**Junfeng Wang,[†] Xiaoyi Wei,[‡] Xiaochu Qin,[§] Xiuping Lin,[†] Xuefeng Zhou,[†] Shengrong Liao,[†] Bin Yang,[†] Juan Liu,[†] Zhengchao Tu,[§] and Yonghong Liu[*,†]**

[†] CAS Key Laboratory of Tropical Marine Bio-resources and Ecology/Guangdong Key Laboratory of Marine Materia Medica/RNAM Center for Marine Microbiology, South China Sea Institute of Oceanology, Chinese Academy of Sciences, Guangzhou 510301, China

[‡] Key Laboratory of Plant Resources Conservation and Sustainable Utilization, South China Botanical Garden, Chinese Academy of Sciences, Guangzhou 510650, China

§ Guangzhou Institutes of Biomedicine and Health, Chinese Academy of Sciences, Guangzhou 510530, China

## List of Supporting Information

**List of contents** **Page**

## Experimental details

**General Experimental Procedures.** Optical rotations were measured with a PerkineElmer 341 polarimeter. UV spectra were recorded on a Shimadzu UV-2401PC spectrometer. IR spectra were measured on JASCO FT/IR-480 plus spectrometer with KBr pellets. $^1H$, $^{13}C$ NMR, DEPT, and 2D-NMR spectra were recorded on the Bruker DRX-500 spectrometer using TMS as internal standard and chemical shifts were recorded as $\delta$-values. HRESIMS (including ESIMS) spectra were recorded on an Applied Biosystems Mariner 5140 spectrometer. X-ray diffraction intensity data were collected on a CrysAlis PRO CCD area detector diffractometer with graphite monochromated Cu Kα radiation (λ= 1.54178Å). TLC and column chromatography (CC) were performed on plates precoated with silica gel $GF_{254}$ (10–40 $\mu$m) and over silica gel (200–300 mesh) (Qingdao Marine Chemical Factory, China), and Sephadex LH-20 (Amersham Biosciences, Sweden), respectively. All solvents used were of analytical grade (Tianjin Fuyu Chemical and Industry Factory). Semipreparative HPLC was performed using an ODS column (YMC-pack ODS-A, 10 × 250 mm, 5 $\mu$m, 4 mL/min).

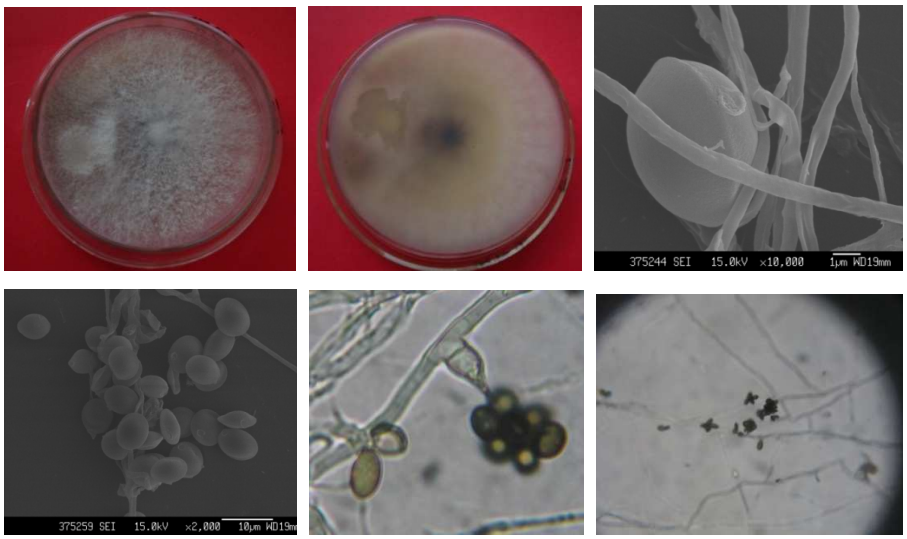

**Figure S1.** Colony appearance and micromorphology of strain *A. arundinis* ZSDS1-F3

**The ITS gene sequence data of *Arthrinium arundinis* ZSDS1-F3**

TCCGTAGGTGAACCTGCGGAGGGATCATTACAGAGTTATACAACTCCCATAC
CATTTGTTAACCTACCCAGTTATGCCTCGGCGTAAGCTCGGTTGGAGGCACCTG
CAGCTACCCTGTAGTTGCACCCGCAGCTACCCTGTAGTTGTTGGTGCAGCTACC
CTGTAGTTGCGGACTGCCAACTCCAGCCGCGGCCCGCCGGCGGTACACTAAAC
TCTGTTTTATTTTATATTCTGAGCGTCTTATTTTAATAAGTTAAAACTTTCAACA
ACGGATCTCTTGGTTCTGGCATCGATGAAGAACGCAGCGAAATGCGATAAGTA
ATGTGAATTGCAGAATTCAGTGAATCATCGAATCTTTGAACGCACATTGCGCCC
ATCAGTATTCTGGTGGGCATGCCTGTTCGAGCGTCATTTCAACCCTTAAGCCTA
GCTTAGTGTTGGGAATCTGCTGTACTGCAGTTCCTTAAAGACAGTGGCGGAGC
GGCGGTAGTCCTCTGAGCGTAGTAATTTATTTCTCGCTTTTGTCAGGCTCTGTCC
TCCCGCCATAAAACCCCCAATTTTTTAGTGGTTGACCTCGGATCAGGTAGGAAT
ACCCGCTGAACTTAAGCATATCAATAA

**Fungal Material.** The fungal strain, *A. arundinis* ZSDS1-F3, was isolated from the sponge *Phakellia fusca Thiele*, which was collected from the Xisha Islands of China in 2012, and identified by Professor Houwen Lin, Second Military Medical University. A voucher specimen (No. 12071301) was deposited in the CAS Key Laboratory of Tropical Marine Bio-resources and Ecology, South China Sea Institute of Oceanology, Chinese Academy of

Sciences, Guangzhou, China. The frozen sample was defrosted in sterile distilled water and washed with sterile distilled water. The washed sample (1 g) was ground with sterile distilled water (10 mL) and then was diluted to $10^{-3}$ g/mL, 100 $\mu$L of which was dispersed across a solid phase agar plate (Czapek's media) and incubated at 28 °C for 7 days. On the marginal zone, gray-white colonies were observed. A single colony was transferred onto Czapek's media. It was identified according to its morphological characteristics (Figure S1) and ITS gene sequences (GenBank Accession No. KF693784). This strain has been deposited in China General Microbiological Culture Collection Center with a deposition number CGMCC 8652. A reference culture is deposited in at our laboratory at –80 °C. The producing strain was prepared on potato dextrose agar slants at 3.3% salt concentration and stored at 4 °C.

**Fermentation and Extraction**. *A*. *arundinis* ZSDS1-F3 was incubated on a rotary shaker (180 rpm) at 28°C for 12 days in 1000 mL × 150 conical flasks containing the liquid medium (300 mL/flask) composed of sorbitol (20 g/L), maltose (20 g/L), MSG (10 g/L), $KH_2PO_4$ (0.5 g/L), $MgSO_4 \cdot 7H_2O$ (0.3 g/L), yeast extract (3 g/L). The fermented whole broth (45 L) was filtered through cheesecloth to separate it into filtrate and mycelia. The filtrate was concentrated under vacuum to about a quarter of original volume and then extracted three times with EtOAc to give an EtOAc solution, while the mycelia were extracted three times with acetone. The acetone solution was evaporated under reduced pressure to afford an aqueous solution. The aqueous solution was extracted three times with EtOAc to give another EtOAc solution. Both EtOAc solutions were combined and concentrated under vacuum to give an EtOAc extract (95.1 g).

**Purification**. The EtOAc extract (95.1 g) was subjected to VLC on a silica gel column using step gradient elution with MeOH–$CH_2Cl_2$ (0–100%) to separate into nine fractions based on TLC properties. Fraction 5 was divided into five parts (Frs.5-1–5-5) by Sephadex LH-20 (MeOH). Compounds **3** (8.0 mg, $t_R$ 20.5 min) was obtained from Fr.5-3 by semipreparative HPLC eluting with 55% Acetonitrile. Fraction 6 was divided into six parts (Frs.6-1–6-6) by Sephadex LH-20 (MeOH). Fr. 6-1 was directly separated by HPLC (72% MeOH/$H_2O$) to yield **1** (28.9 mg, $t_R$ 19.8 min). Fraction 7 was divided into six parts (Frs.7-1–7-6) by Sephadex LH-20 (MeOH). Fr. 7-2 was further divided into six parts

(Frs.7-2-1–7-2-6) by HPLC (50% Acetonitrile/$H_2O$). Fr. 7-2-1 was purified by HPLC (40% Acetonitrile/$H_2O$) to yield **2** (6.4 mg, $t_R$ 7.6 min). Fr. 7-2-4 was purified by HPLC (75% MeOH/$H_2O$) to yield **4** (533.2 mg, $t_R$ 17.6 min).

**Arthpyrone A (1):** yellow amorphous solid; $[\alpha]_D^{25}$ –4.2 (*c* 2.9, MeOH); UV (MeOH) $\lambda_{max}$ (log $\varepsilon$): 207 (3.65), 274 (2.82), 320 (2.95) nm; IR (KBr) $\nu_{max}$ 3321, 1682, 1639, 1535, 1431, 1373, 1204, 1138, 1111, 1026 $cm^{-1}$; $^1H$ NMR and $^{13}C$ NMR data, see Table 1; HRESIMS *m*/*z* 446.2169 $[M + H]^+$ (calcd for $C_{24}H_{32}NO_7$, 446.2173).

**Arthpyrone B (2):** yellow amorphous solid; $[\alpha]_D^{25}$ –7.0 (*c* 0.6, MeOH); UV (MeOH) $\lambda_{max}$ (log $\varepsilon$): 202 (3.39), 219 (3.39), 311 (2.78) nm; IR (KBr) $\nu_{max}$ 3460, 1690, 1643, 1531, 1435, 1315, 1207, 1134, 1096, 1038 $cm^{-1}$; $^1H$ NMR and $^{13}C$ NMR data, see Table 1; HRESIMS *m*/*z* 428.2069 $[M - H]^-$ (calcd for $C_{24}H_{30}NO_6$, 428.2079).

**Arthpyrone C (3):** yellow amorphous solid; $[\alpha]_D^{25}$ –68.0 (*c* 0.7, MeOH); UV (MeOH) $\lambda_{max}$ (log $\varepsilon$): 204 (3.56), 287 (3.12), 339 (2.94) nm; IR (KBr) $\nu_{max}$ 1639, 1605, 1531, 1435, 1373, 1265, 1215, 1099, 1057 $cm^{-1}$; $^1H$ NMR and $^{13}C$ NMR data, see Table 1; HRESIMS *m*/*z* 460.2320 $[M + H]^+$ (calcd for $C_{25}H_{34}NO_7$, 460.2330).

**Table S1**. Cytotoxicities against Tumor Cells for **1**–**4**.

| Cell lines | $IC_{50}$ ($\mu$M) | | | | |
|---|---|---|---|---|---|
| | **1** | **2** | **3** | **4** | TSA |
| K562 | >50 | >50 | 3.5 | 0.45 | 0.16 |
| MOLT-4 | 22 | >50 | 0.87 | 0.66 | 0.034 |
| U937 | 31 | >50 | 1.3 | 0.24 | 0.059 |
| MCF-7 | >50 | >50 | 5.6 | 0.99 | 0.079 |
| Hela | >50 | >50 | 2.1 | 1.3 | 0.10 |
| Huh-7 | >50 | >50 | 11 | 2.2 | 0.089 |
| A549 | >50 | >50 | 8.1 | 1.7 | 0.053 |
| BGC823 | >50 | >50 | 7.6 | 1.3 | 0.081 |
| H1975 | 45 | >50 | 8.6 | 1.6 | 0.099 |
| HL60 | >50 | >50 | 1.3 | 0.89 | 0.082 |

**Table S2.** Anti-AchE activities of **1**–**4**.

| Activity | $IC_{50}$ ($\mu$M) | | | | |
|---|---|---|---|---|---|
| | **1** | **2** | **3** | **4** | Tacrine |
| Anti-AchE | 47 | >100 | 0.81 | 39 | 0.48 |

**Cytotoxicity Assay.** Cytotoxicity was assayed with the CCK-8 (Dojindo, Japan) method. Cell lines, K562, A549, Huh-7, H1975, MCF-7, U937, BGC823, HL60, Hela, and MOLT-4 were purchased from Shanghai Cell Bank, Chinese Academy of Sciences. Cells were routinely grown and maintained in mediums RPMI or DMEM with 10% FBS and with 1% penicillin/streptomycin. All cell lines were incubated in a Thermo/Forma Scientific $CO_2$ Water Jacketed Incubator with 5% $CO_2$ in air at 37 °C. Cell viability assay was determined by the CCK-8 (Dojindo, Japan) assay. Cells were seeded at a density of 400-800 cells/well in 384 well plates and treated with various concentration of compounds or solvent control. After 72 h incubation, CCK-8 reagent was added, and absorbance was measured at 450 nm using Envision 2104 multi-label Reader (Perkin Elmer, USA). Dose response curves were plotted to determine the $IC_{50}$ values using Prism 5.0 (GraphPad Software Inc., USA). TSA was used as the positive control.

**AchE inhibitory Assay.** The AchE inhibitory activity was measured according to Ellman's coupled enzyme assay, modified as follow. 0.2Units of AchE were dissolved in 0.1M potassium phosphate buffer (pH 7.4), and purified compounds dissolved in DMSO (the series of final concentrations as 8, 4, 2, 1, 0.5, 0.25 $\mu$M) were added to each well of a 96-well plate. Then, acetylthiocholine iodide and 5,5'-dithiobis(2-nitrobenzoic acid) dissolved in 0.1M potassium phosphate buffer (pH 7.4) were added to reach a final concentration of 50 $\mu$M both. The reaction was carried out at 30□ for 30 min. The absorbance was measured at 410 nm using a spectrophotometer and the half maximum inhibitory concentration ($IC_{50}$) was calculated. Tacrine was used as the positive control with an $IC_{50}$ value of 0.48 $\mu$M.

## Computational Details

### 1. Methods

Molecular Merck force field (MMFF) and DFT/TDDFT calculations were performed with Spartan' 14 software package (Wavefunction Inc., Irvine, CA, USA) and Gaussian09 program package,[1] respectively, using default grids and convergence criteria. MMFF conformational search generated low-energy conformers within a 10 kcal/mol energy window were subjected to geometry optimization using DFT method at the B3LYP/6-31G (d) level. Frequency calculations were run at the same level to verify that each optimized conformer was a true minimum and to estimate their relative thermal free energies ($\Delta G$) at 298.15K. Energies of the low-energy conformers in MeOH were calculated at the B3LYP/6-311+G (d,p) level. Solvent effects were taken into account by using polarizable continuum model (PCM). The TDDFT calculations were performed using the long-range corrected hybrid CAM-B3LYP and the hybrid B3LYP functionals, and Ahlrichs' basis sets SVP (split valence plus polarization)[2] and TZVP (triple zeta valence plus polarization).[3] The number of excited states per each molecule was 36. The CD spectra were generated by the program SpecDis[4] using a Gaussian band shape with 0.23–0.45 eV exponential half-width from dipole-length dipolar and rotational strengths; the difference with dipole-velocity values was negligible (<10%) for most transitions. Equilibrium population of each conformer at 298.15K was calculated from its relative free energies using Boltzmann statistics. The calculated spectra of compounds **1**–**4** were generated from the low-energy conformers according to the Boltzmann weighting of each conformer in MeOH solution.

## 2. Results

**Table S3.** Relative and free energies[a] and equilibrium populations[b] of low-energy conformers of **1**−**4** in MeOH.

| conformer | $\Delta E$ | $\Delta G$ | P (%) |
|---|---|---|---|
| Compound **1** | | | |
| **1a** | 0.00 | 0.00 | 76.7 |
| **1b** | 1.23 | 0.92 | 15.8 |
| **1c** | 1.59 | 1.73 | 3.9 |
| **1d** | 1.66 | 1.79 | 3.5 |
| Compound **2** | | | |
| **2a** | 0.00 | 0.00 | 73.9 |
| **2b** | 1.21 | 0.95 | 14.9 |
| **2c** | 1.42 | 1.46 | 6.3 |
| **2d** | 1.51 | 1.61 | 4.9 |
| Compound **3** | | | |
| **4a** | 0.00 | 0.00 | 64.4 |
| **4b** | 0.63 | 0.44 | 30.6 |
| **4c** | 1.28 | 1.55 | 4.7 |
| **4d**[c] | 3.15 | 3.13 | 0.3 |
| Compound **4** | | | |
| **5a** | 0.00 | 0.00 | 39.9 |
| **5b** | 0.45 | 0.20 | 28.5 |
| **5c** | 0.36 | 0.40 | 20.2 |
| **5d** | 1.10 | 0.74 | 11.4 |

[a]At the B3LYP/6-311+G(d,p) level, in kcal/mol. [b]From $\Delta G$ values at 298.15 K. [c]Conformer not used for ECD/TDDFT calculations.

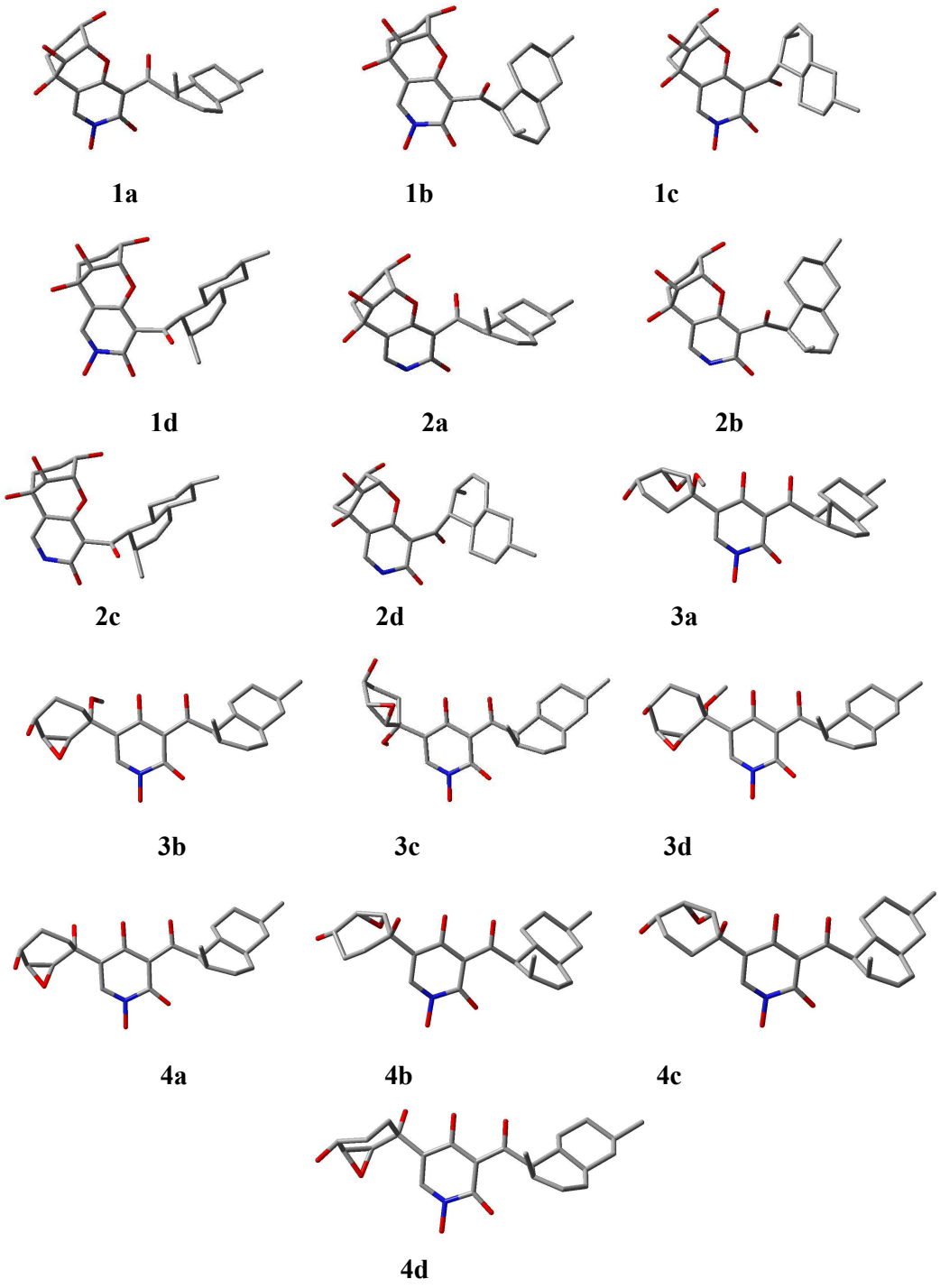


**Figure S2.** Conformations of low-energy conformers of **1**–**4**.

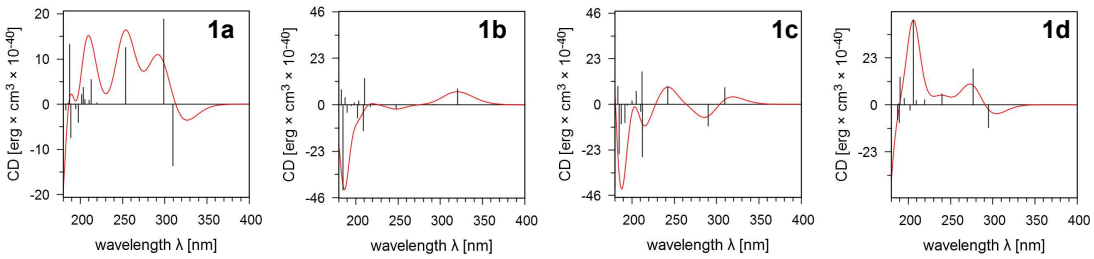


**Figure S3.** Calculated ECD spectra of the low-energy conformers of **1** in MeOH using the CAM-B3LYP/SVP method. Vertical bars represent rotational strengths *R*. σ = 0.30 eV; shift = ±0 nm.

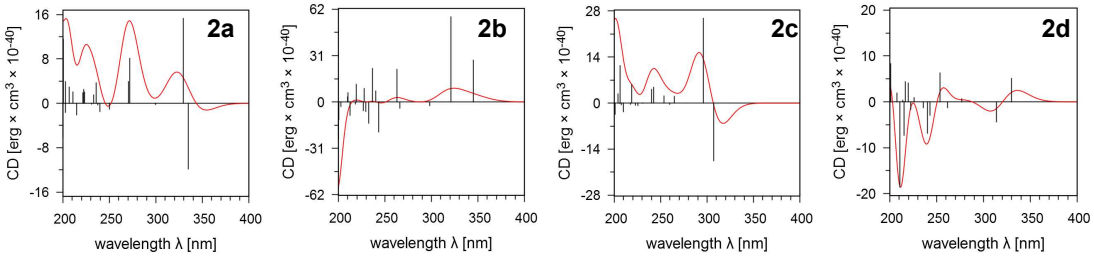


**Figure S4.** Calculated ECD spectra of the low-energy conformers of **2** in MeOH using the B3LYP/TZVP method. Vertical bars represent rotational strengths *R*. σ = 0.23 eV; shift = ±0 nm.

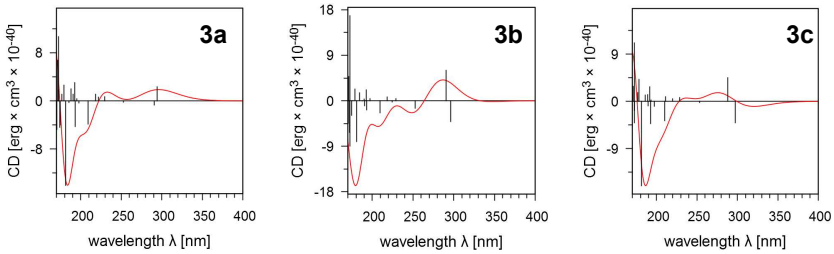


**Figure S5.** Calculated ECD spectra of the low-energy conformers of **3** in MeOH using the CAM-B3LYP/SVP method. Vertical bars represent rotational strengths *R*. σ = 0.45 eV; shift = ±0 nm.

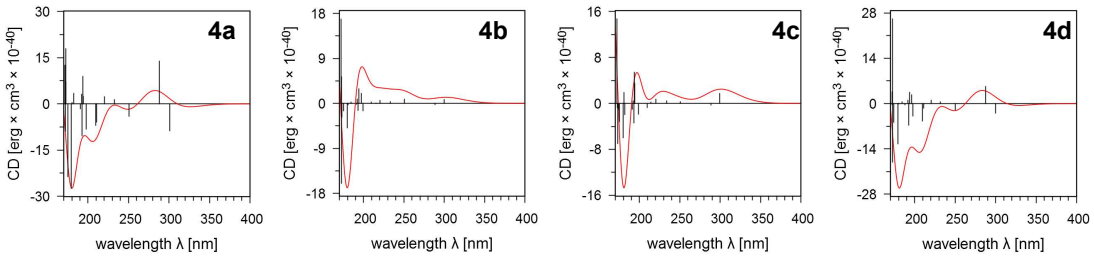


**Figure S6.** Calculated ECD spectra of the low-energy conformers of **4** in MeOH using the CAM-B3LYP/SVP method. Vertical bars represent rotational strengths *R*. σ = 0.40 eV; shift = ±0 nm.

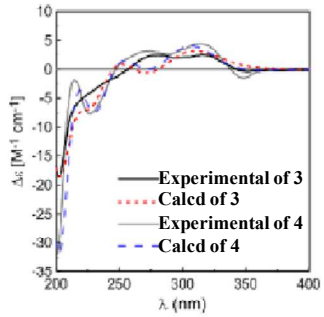


**Figure S7.** Comparison between calculated (CAM-B3LYP/SVP) and experimental ECD spectra of **3** and **4** in MeOH.

## 3. References

(1) Frisch, M. J.; Trucks, G. W.; Schlegel, H. B.; Scuseria, G. E.; Robb, M. A.; Cheeseman, J. R.; Scalmani, G.; Barone, V.; Mennucci, B.; Petersson, G. A.; Nakatsuji, H.; Caricato, M.; Li, X.; Hratchian, H. P.; Izmaylov, A. F.; Bloino, J.; Zheng, G.; Sonnenberg, J. L.; Hada, M.; Ehara, M.; Toyota, K.; Fukuda, R.; Hasegawa, J.; Ishida, M.; Nakajima, T.; Honda, Y.; Kitao, O.; Nakai, H.; Vreven, T.; Montgomery, J. A.; Peralta, J. E.; Ogliaro, F.; Bearpark, M.; Heyd, J. J.; Brothers, E.; Kudin, K. N.; Staroverov, V. N.; Keith, T.; Kobayashi, R.; Normand, J.; Raghavachari, K.; Rendell, A.; Burant, J. C.; Iyengar, S. S.; Tomasi, J.; Cossi, M.; Rega, N.; Millam, J. M.; Klene, M.; Knox, J. E.; Cross, J. B.; Bakken, V.; Adamo, C.; Jaramillo, J.; Gomperts, R.; Stratmann, R. E.; Yazyev, O.; Austin, A. J.; Cammi, R.; Pomelli, C.; Ochterski, J. W.; Martin, R. L.; Morokuma, K.; Zakrzewski, V. G.; Voth, G. A.; Salvador, P.; Dannenberg, J. J.; Dapprich, S.; Daniels, A. D.; Farkas, O.; Foresman, J. B.; Ortiz, J. V.; Cioslowski, J.; Fox, D. J. Gaussian 09, revision C.01. Gaussian, Inc.: Wallingford CT, **2010**.

(2) Schäfer, A.; Horn, H.; Ahlrichs, R. *J. Chem. Phys.* **1992**, *97*, 2571–2577.

(3) Schäfer, A.; Huber, C.; Ahlrichs, R. *J. Chem. Phys.* **1994**, *100*, 5829–5835.

(4) Bruhn, T.; Schaumlöffel, A.; Hemberger, Y.; Bringmann, G. SpecDis Version 1.60. Germany: University of Wuerzburg; **2012**.

**Figure S8**. The $^{1}H$ NMR spectrum of arthpyrone A (**1**) in $CD_3OD$

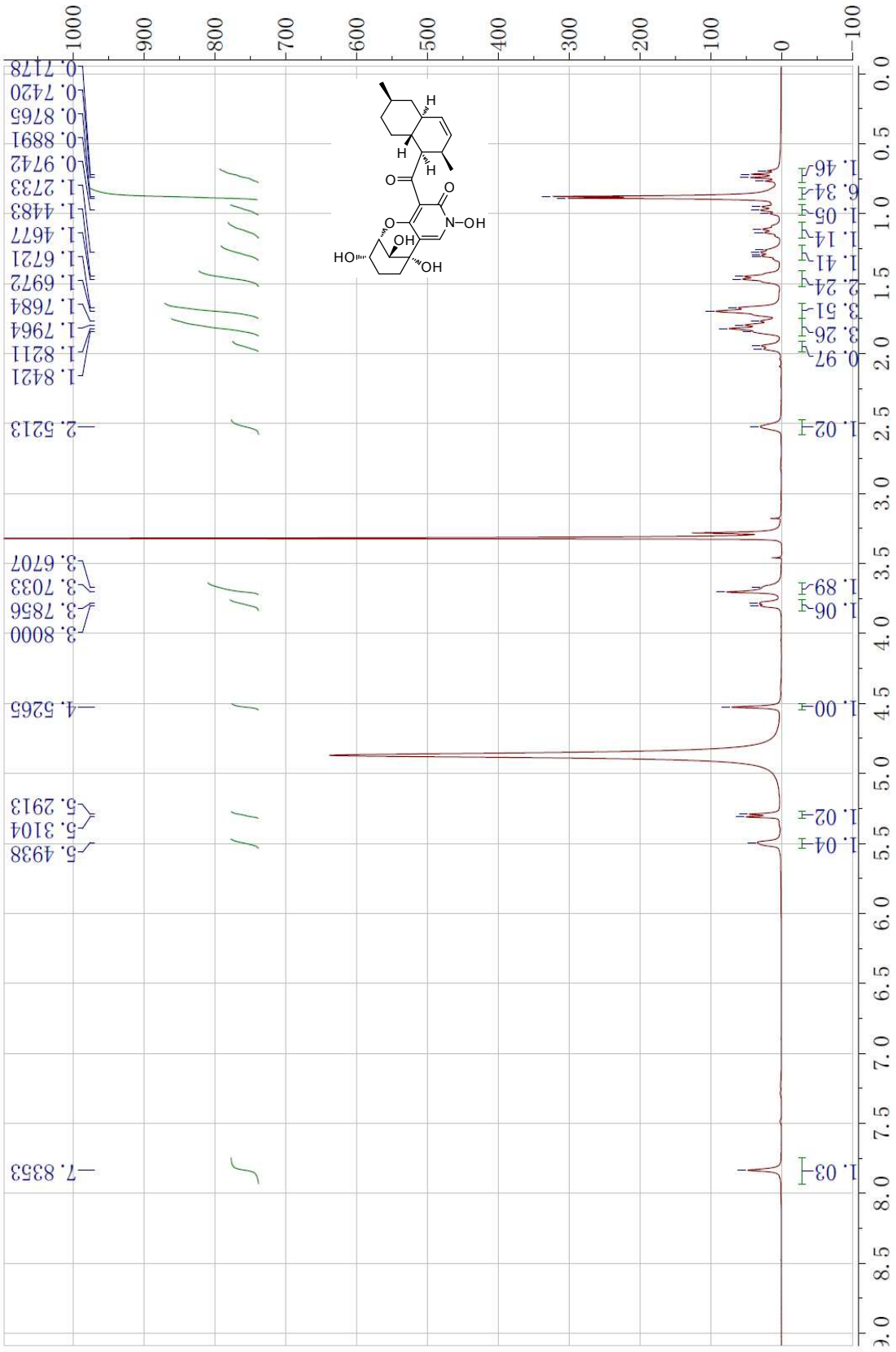

**Figure S9**. The $^{13}C$ NMR spectrum of arthpyrone A (**1**) in $CD_3OD$

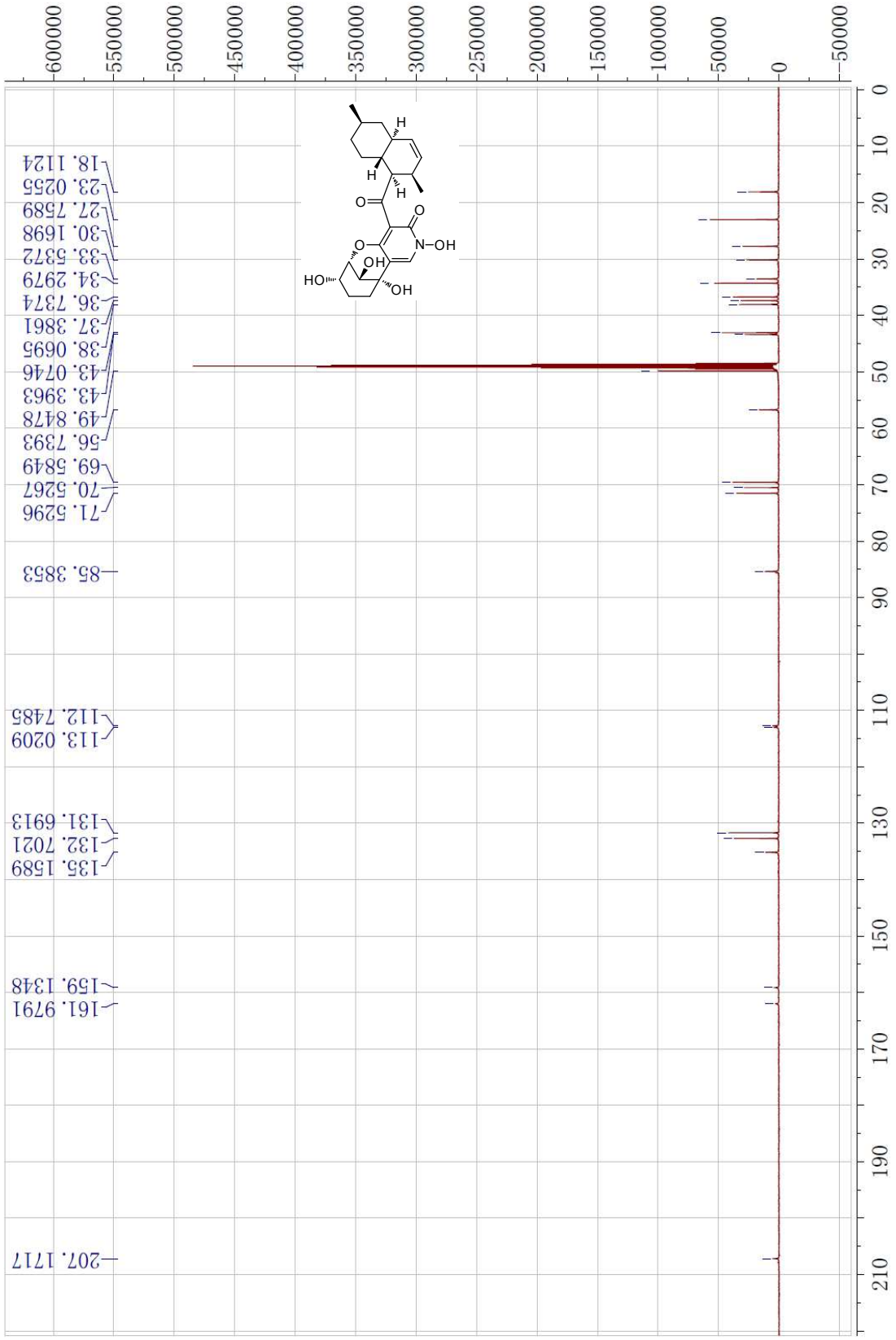

**Figure S10**. The HMQC spectrum of arthpyrone A (**1**) in $CD_3OD$

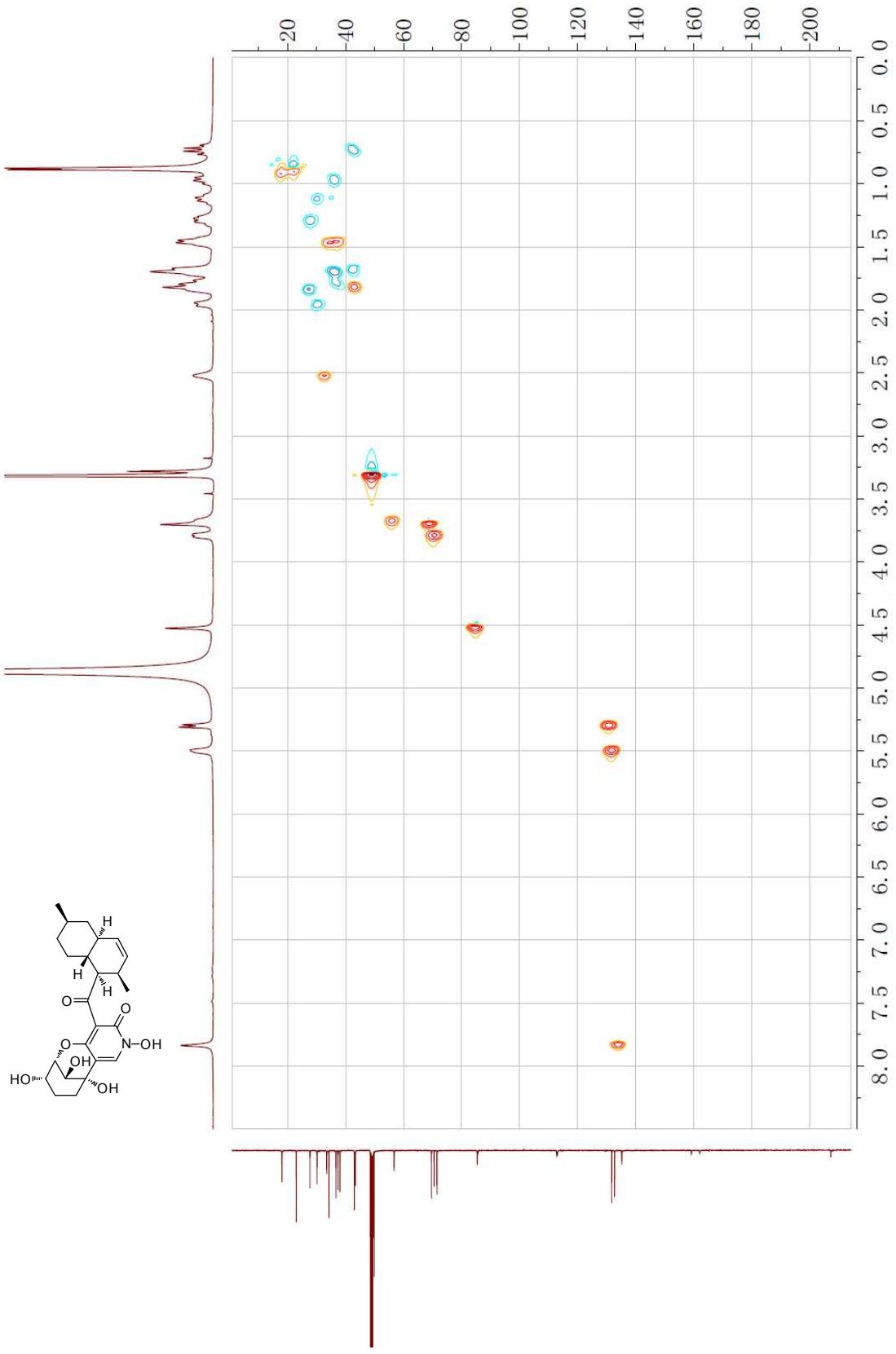

**Figure S11**. The $^{1}H$-$^{1}H$ COSY spectrum of arthpyrone A (**1**) in $CD_3OD$

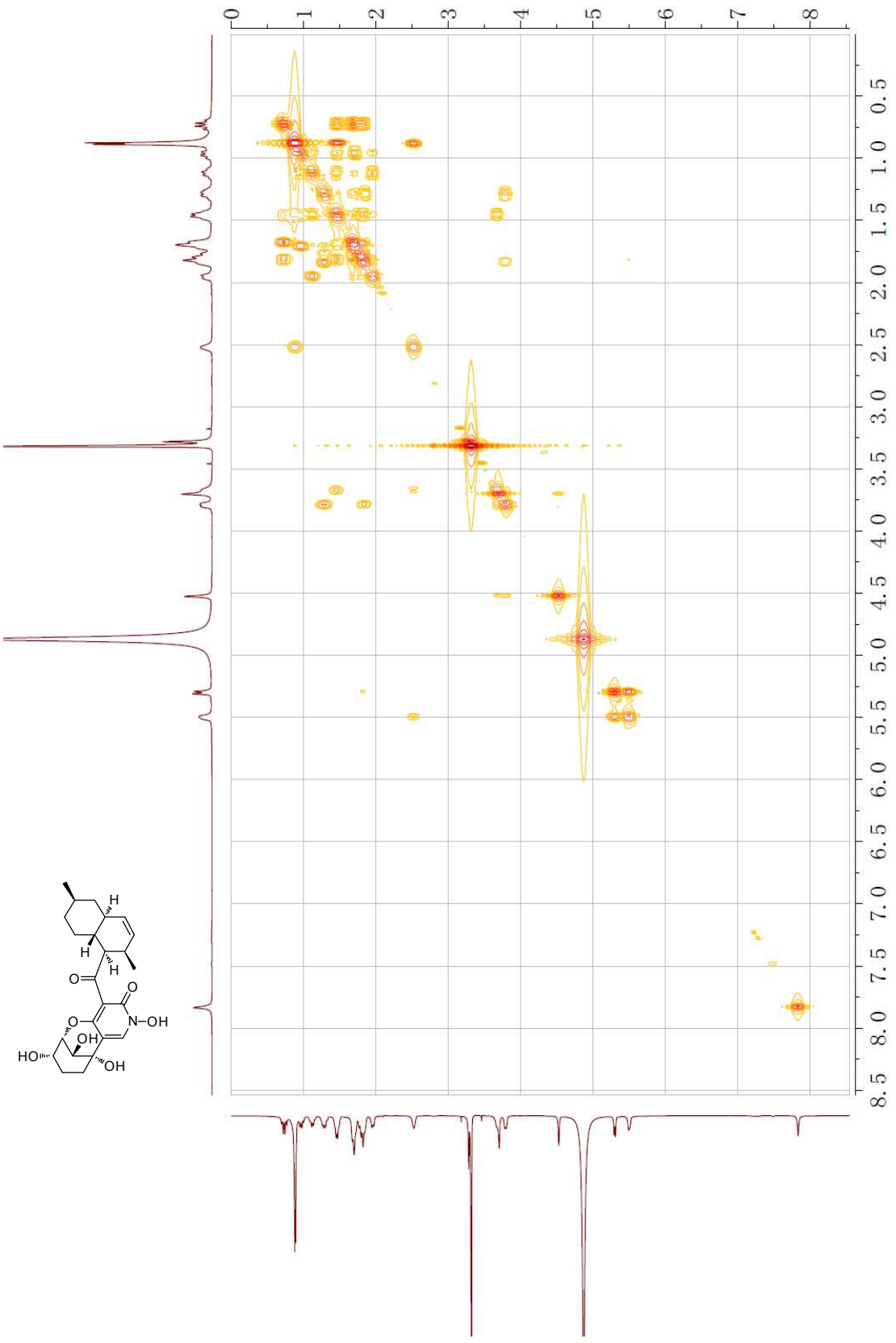

**Figure S12**. The HMBC spectrum of arthpyrone A (**1**) in $CD_3OD$

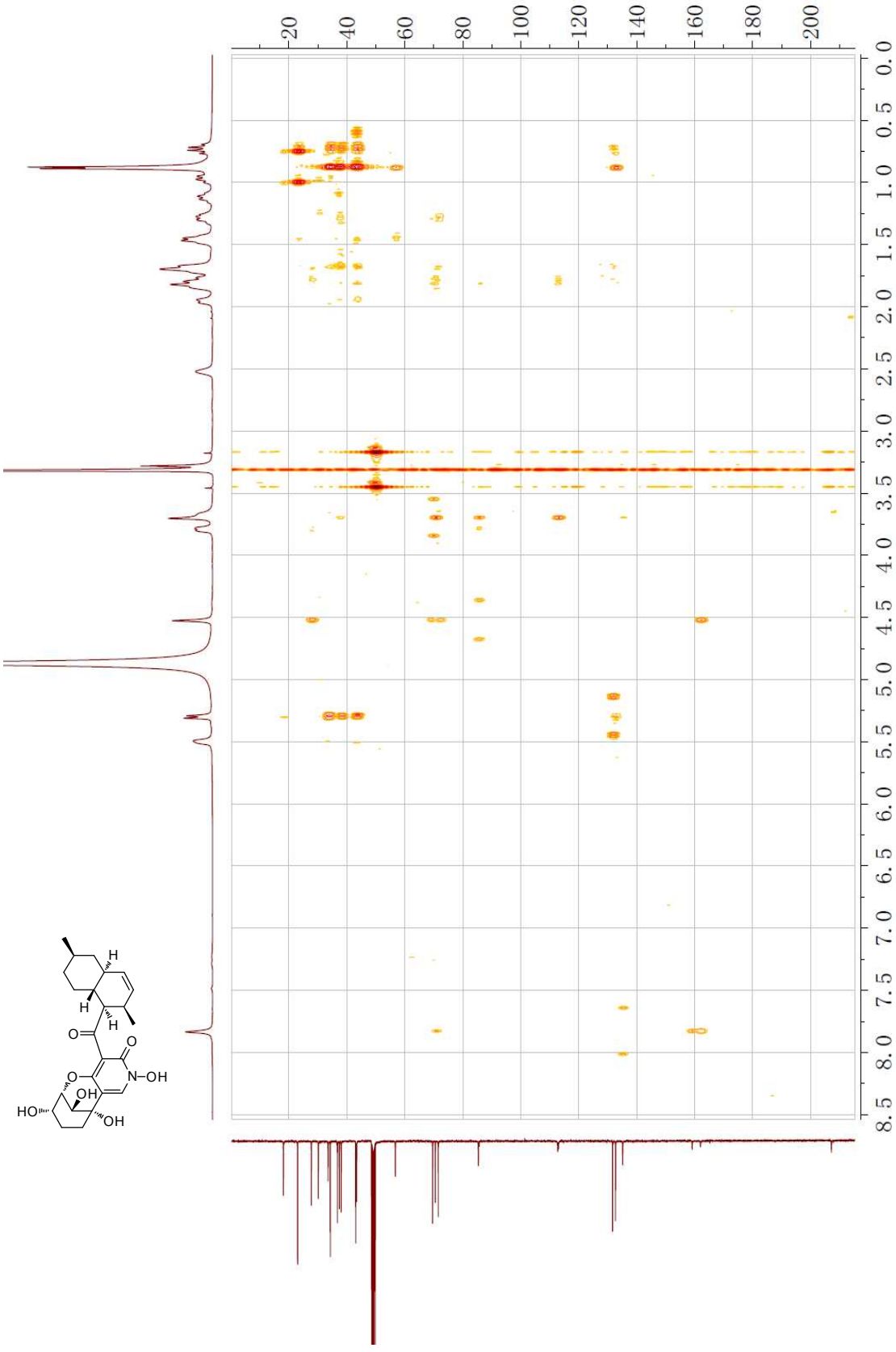

**Figure S13**. The NOESY spectrum of arthpyrone A (**1**) in $CD_3OD$

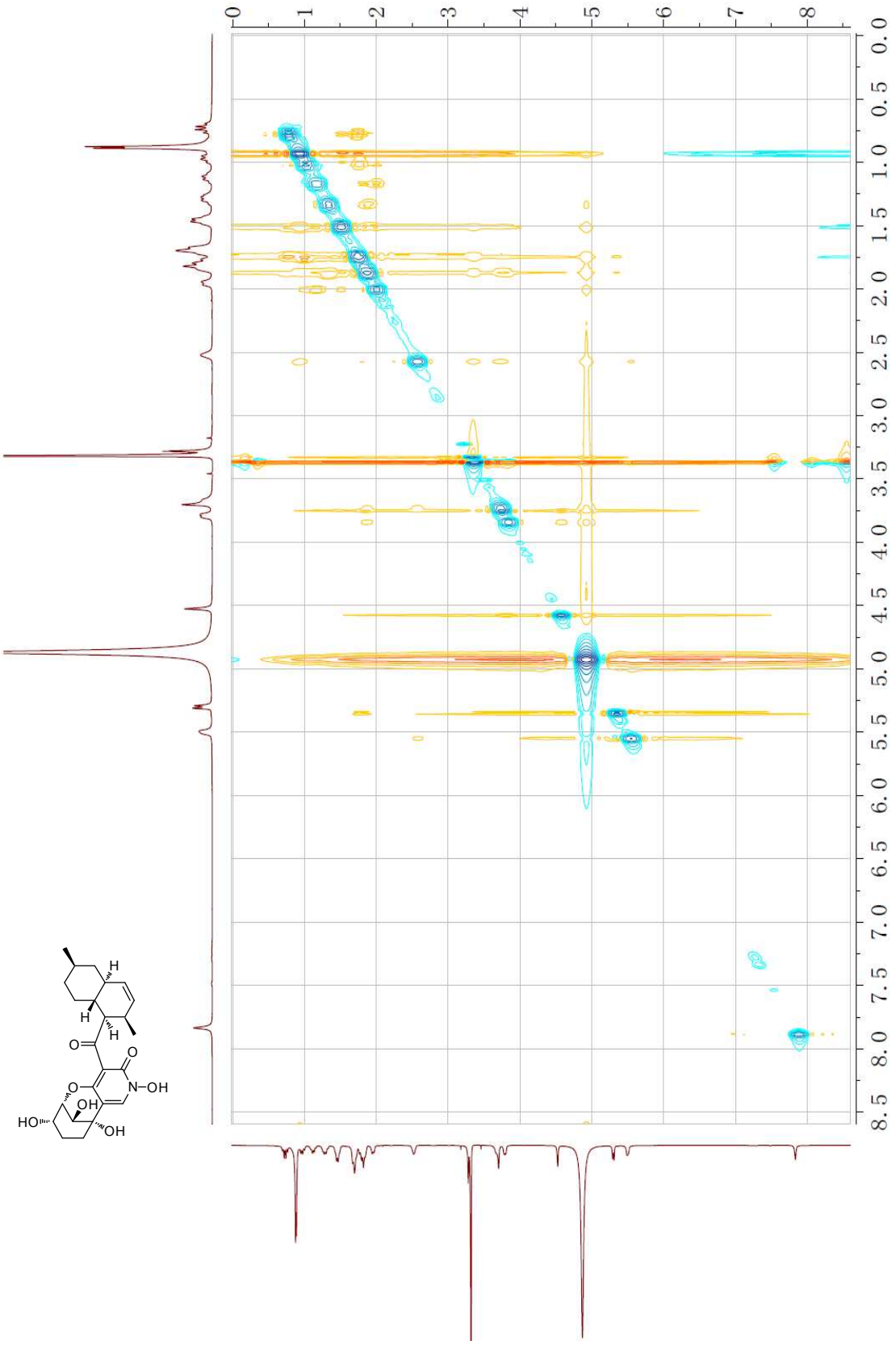

**Figure S14**. The HRESIMS spectrum of arthpyrone A (**1**)

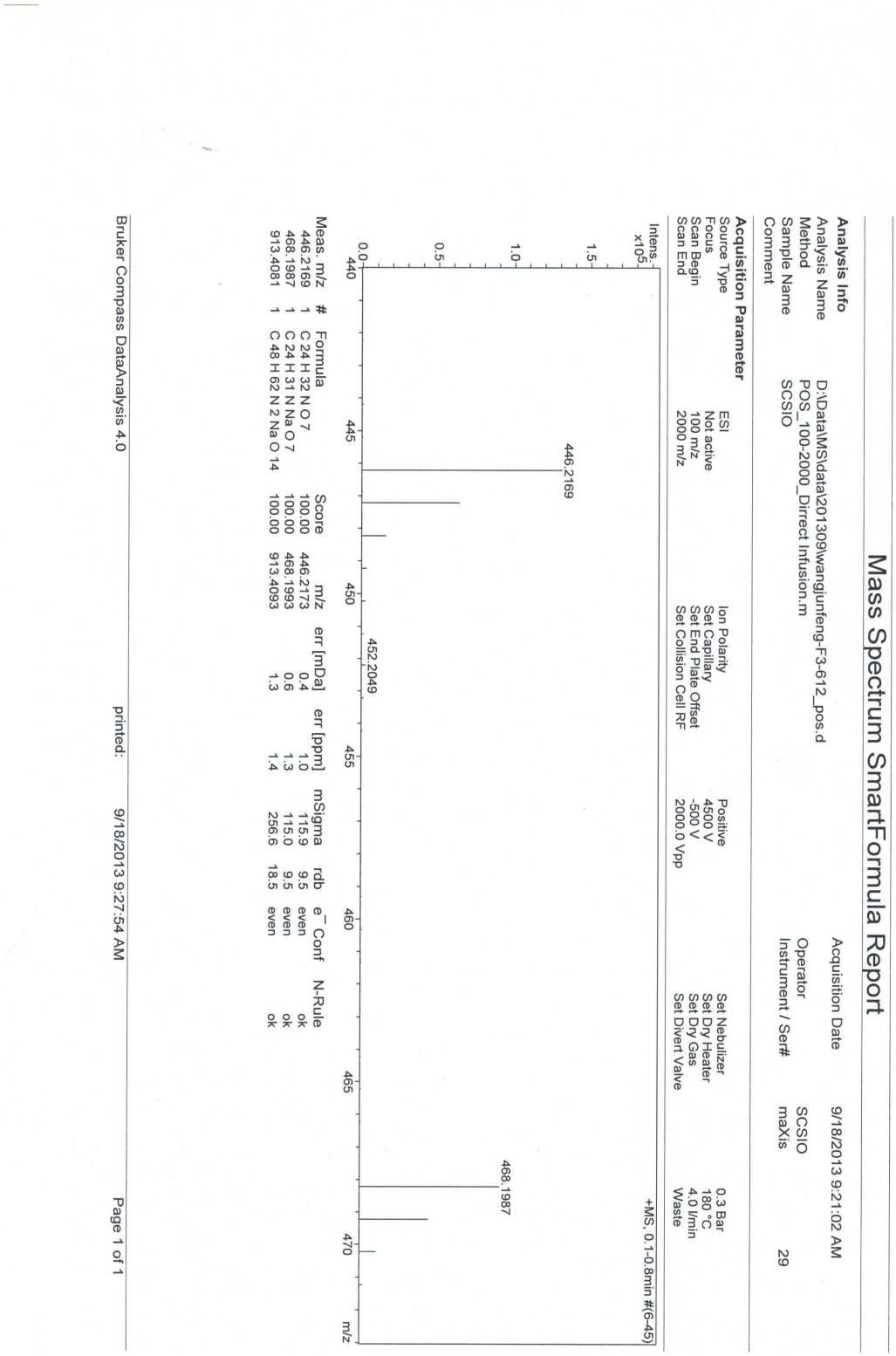

Mass Spectrum SmartFormula Report

**Analysis Info**

| | | | |
|---|---|---|---|
| Analysis Name | D:\DataMS\data\201309\wangjunfeng-F3-612_pos.d | Acquisition Date | 9/18/2013 9:21:02 AM |
| Method | POS_100-2000_Dirrect Infusion.m | Operator | SCSIO |
| Sample Name | SCSIO | Instrument / Ser# | maXis 29 |
| Comment | | | |

**Acquisition Parameter**

| | | | | | |
|---|---|---|---|---|---|
| Source Type | ESI | Ion Polarity | Positive | Set Nebulizer | 0.3 Bar |
| Focus | Not active | Set Capillary | 4500 V | Set Dry Heater | 180 °C |
| Scan Begin | 100 m/z | Set End Plate Offset | -500 V | Set Dry Gas | 4.0 l/min |
| Scan End | 2000 m/z | Set Collision Cell RF | 2000.0 Vpp | Set Divert Valve | Waste |



| Meas. m/z | # | Formula | Score | m/z | err [mDa] | err [ppm] | mSigma | rdb | e⁻ Conf | N-Rule |
|---|---|---|---|---|---|---|---|---|---|---|
| 446.2169 | 1 | C 24 H 32 N O 7 | 100.00 | 446.2173 | 0.4 | 1.0 | 115.9 | 9.5 | even | ok |
| 468.1987 | 1 | C 24 H 31 N Na O 7 | 100.00 | 468.1993 | 0.6 | 1.3 | 115.0 | 9.5 | even | ok |
| 913.4081 | 1 | C 48 H 62 N 2 Na O 14 | 100.00 | 913.4093 | 1.3 | 1.4 | 256.6 | 18.5 | even | ok |

**Figure S15**. The $^{1}H$ NMR spectrum of arthpyrone B (**2**) in $CD_3OD$

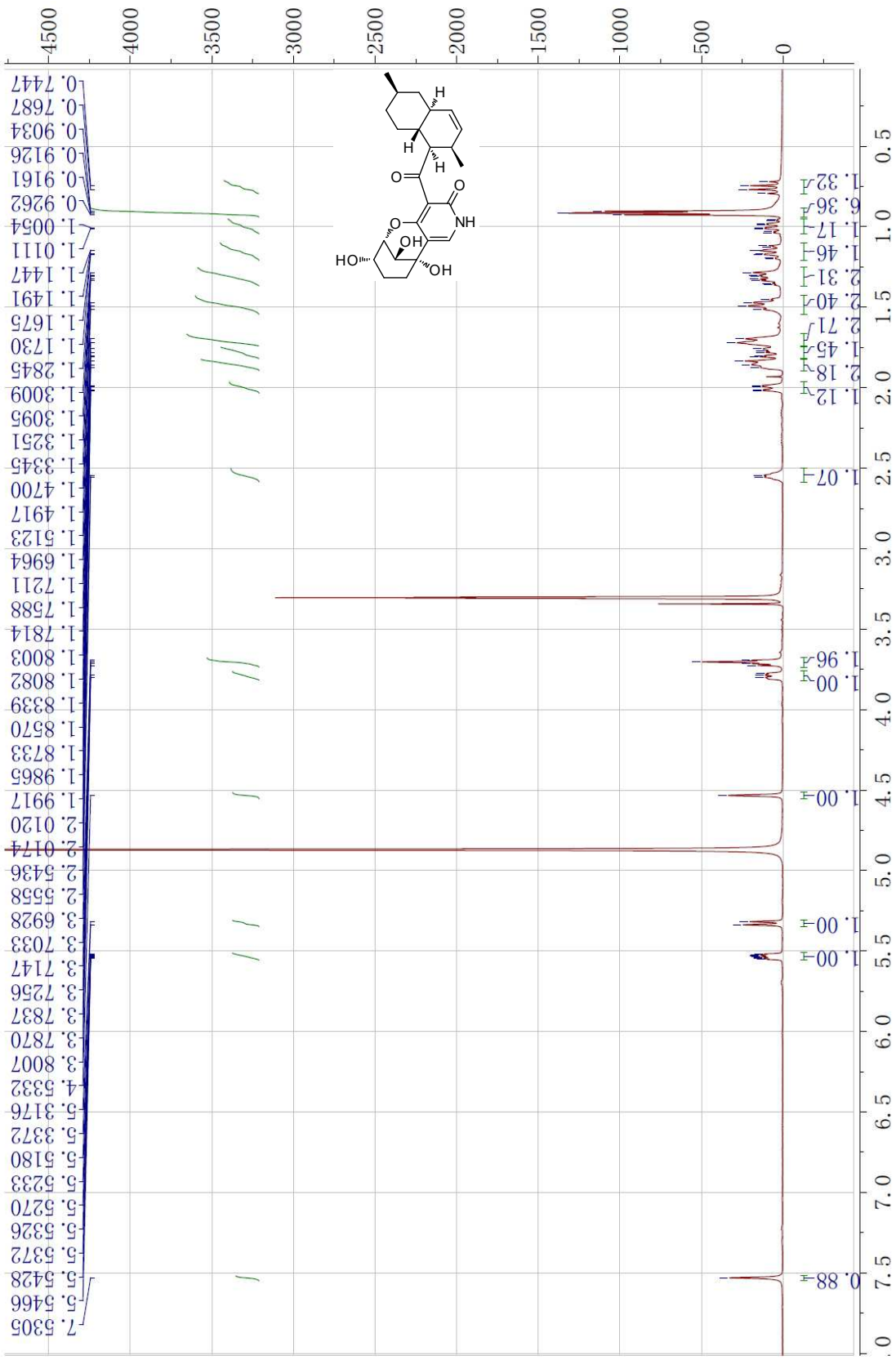

**Figure S16**. The $^{13}C$ NMR spectrum of arthpyrone B (**2**) in $CD_3OD$

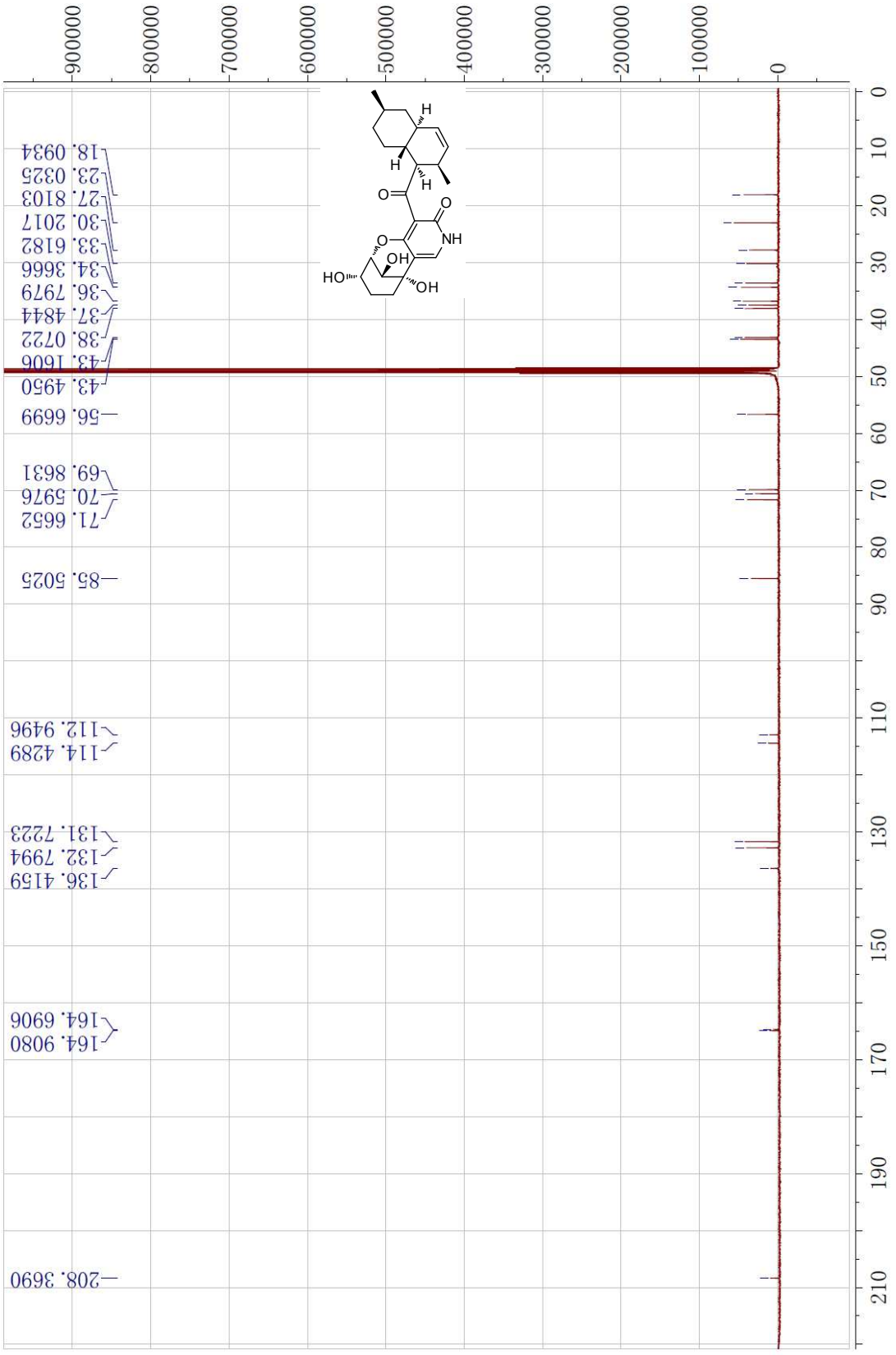

**Figure S17**. The HMQC spectrum of arthpyrone B (**2**) in $CD_3OD$

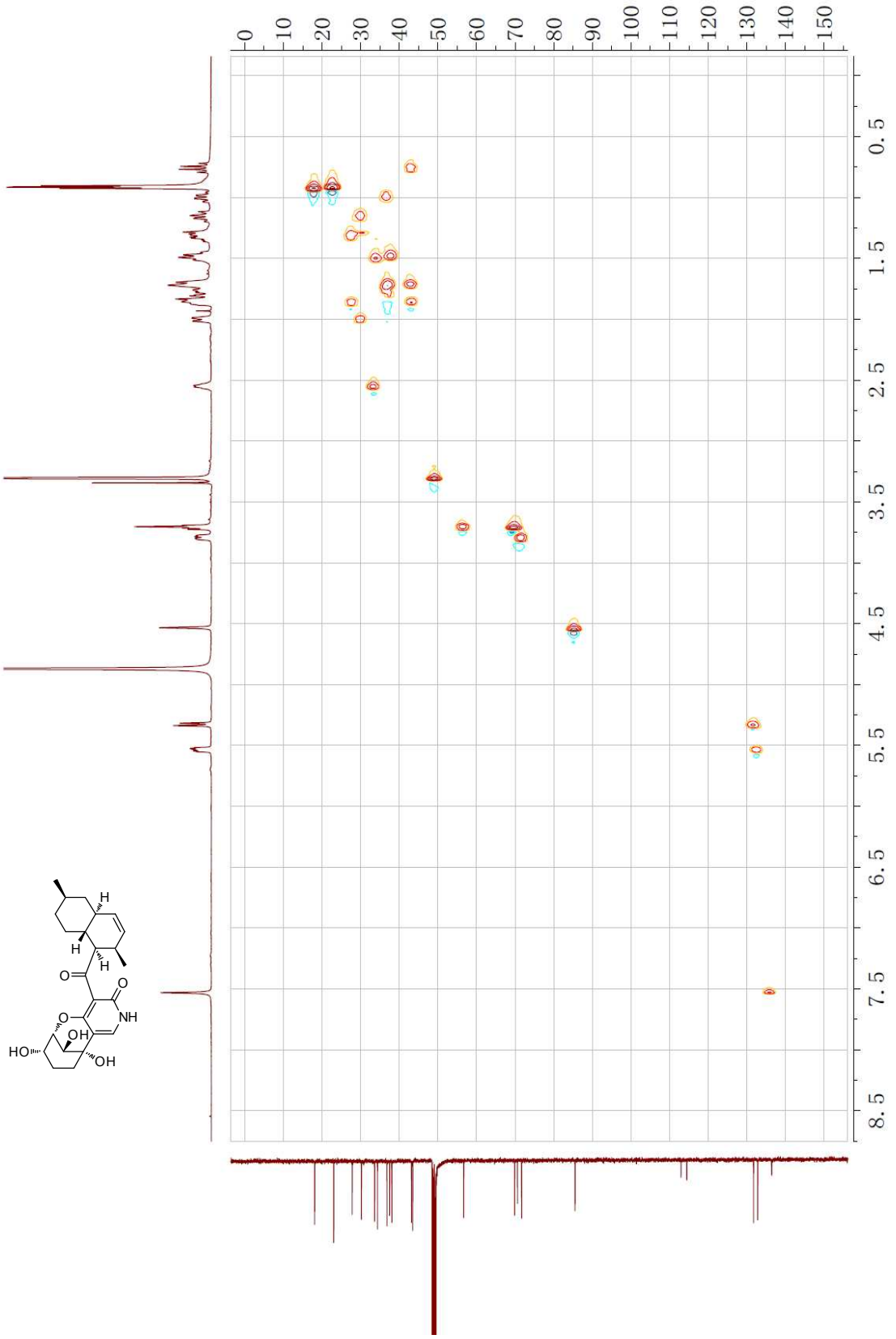

**Figure S18**. The $^{1}H$-$^{1}H$ COSY spectrum of arthpyrone B (**2**) in $CD_3OD$

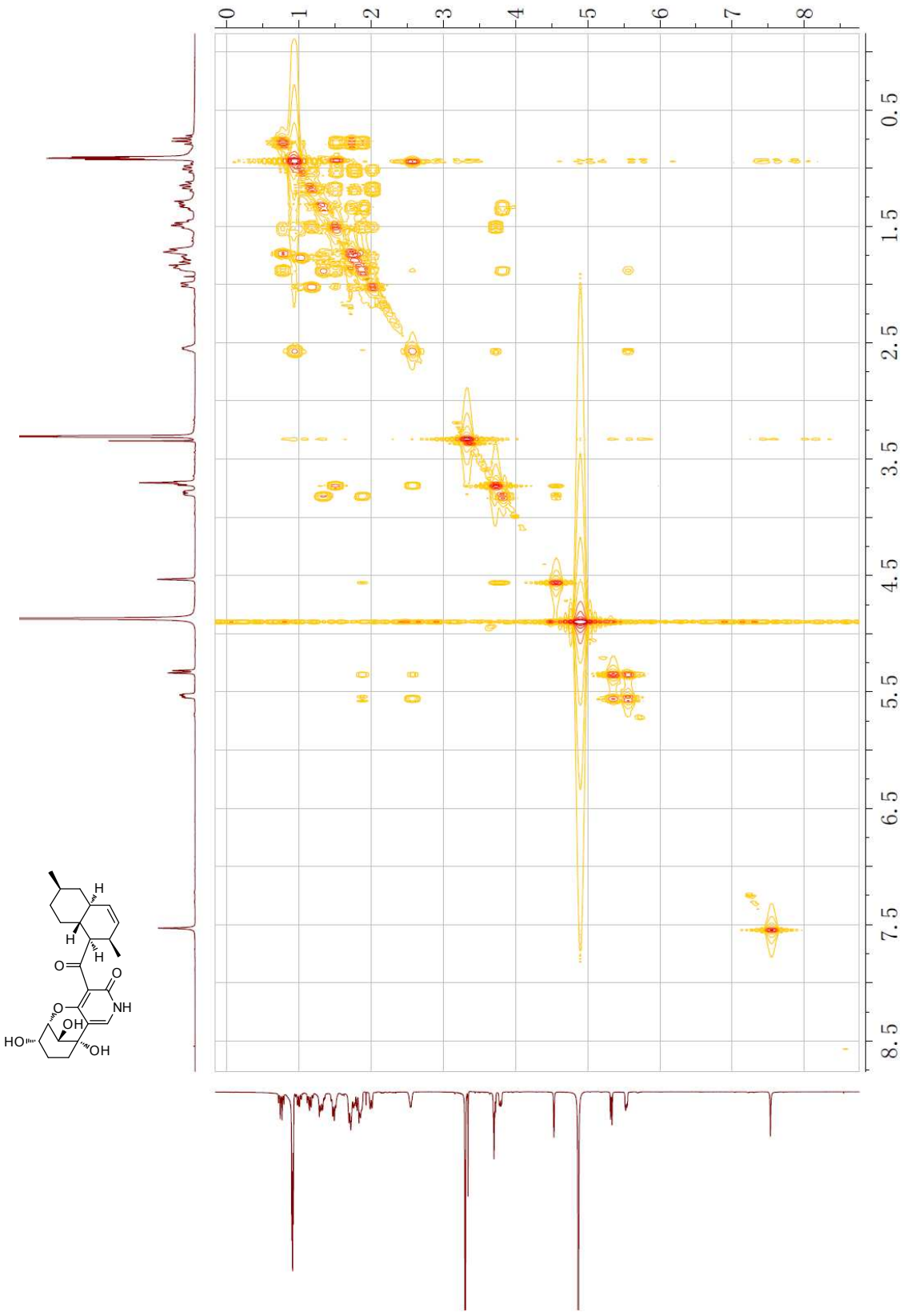

**Figure S19**. The HMBC spectrum of arthpyrone B (**2**) in $CD_3OD$

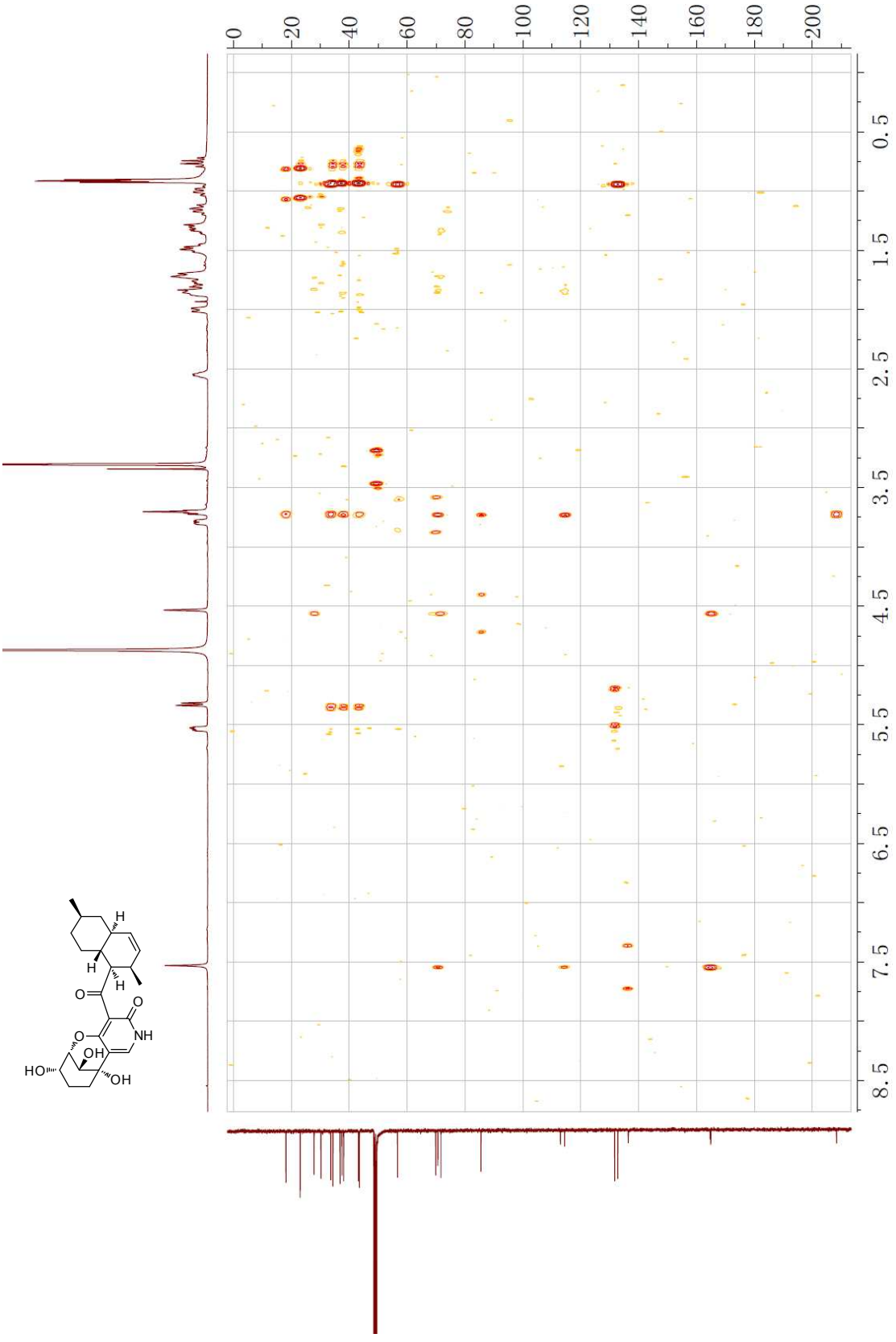

**Figure S20**. The NOESY spectrum of arthpyrone B (**2**) in $CD_3OD$

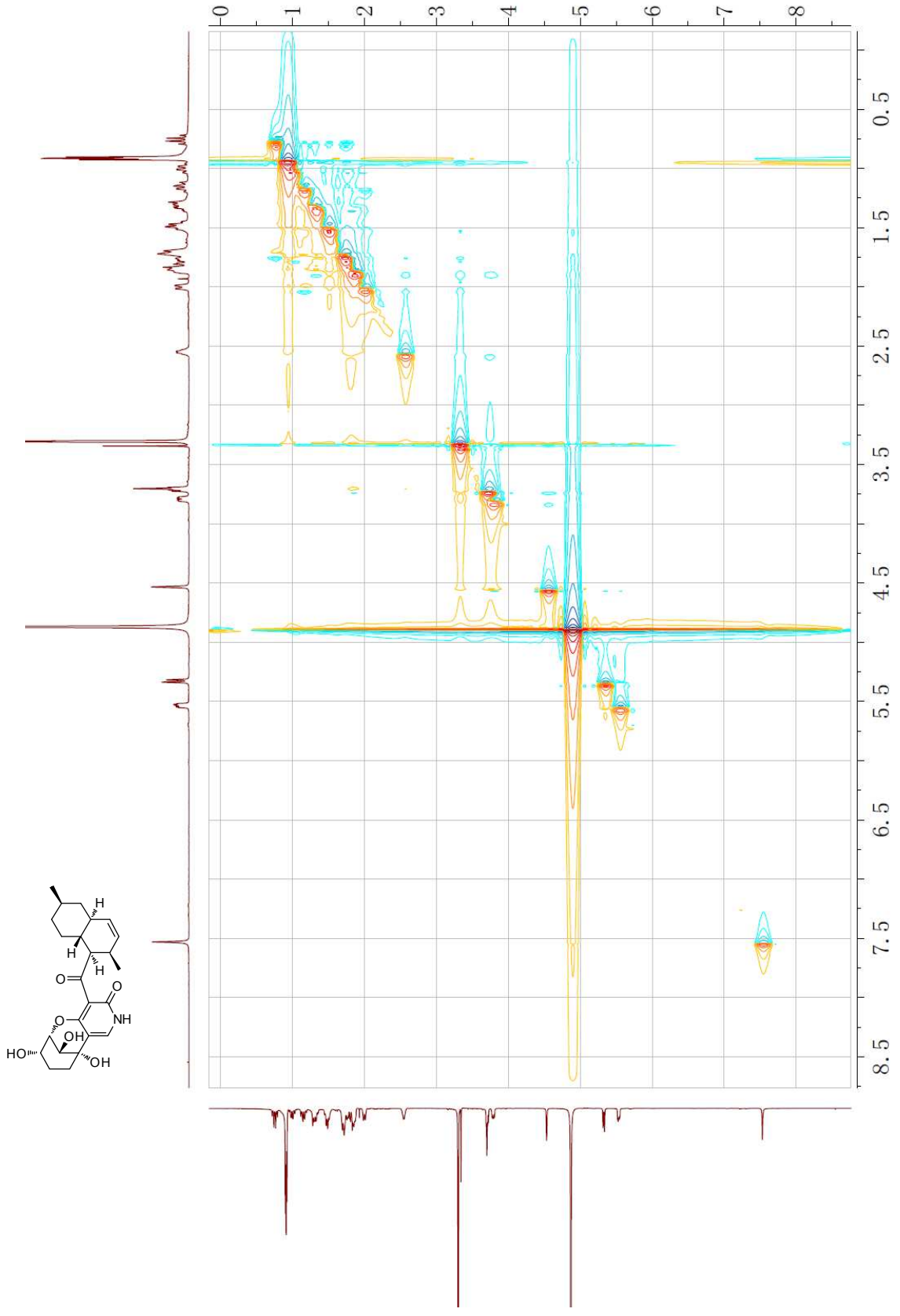

**Figure S21**. The HRESIMS spectrum of arthpyrone B (**2**)

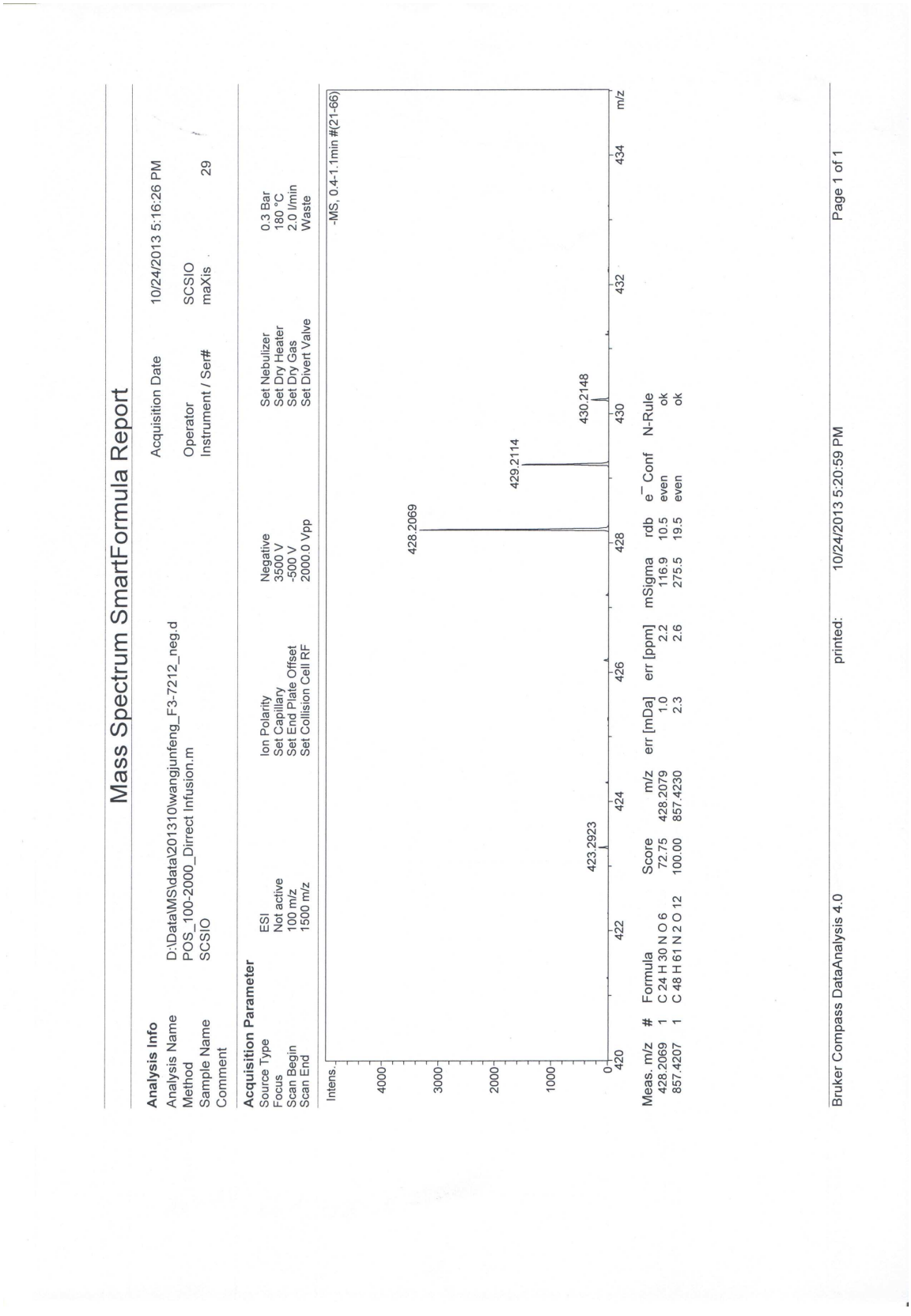

**Figure S22**. The $^{1}H$ NMR spectrum of arthpyrone C (**3**) in $CD_3OD$

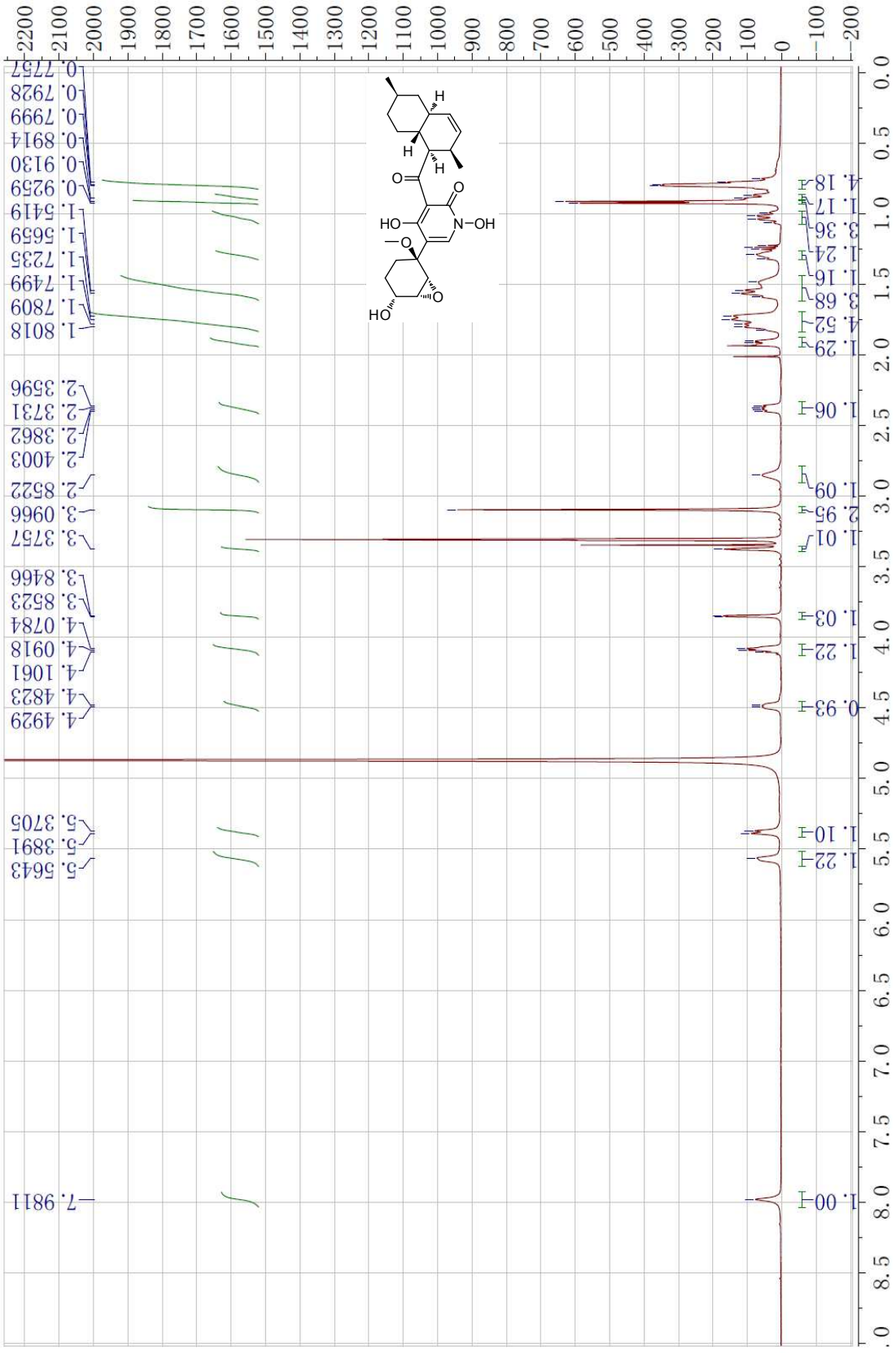

**Figure S23**. The $^{13}C$ NMR spectrum of arthpyrone C (**3**) in $CD_3OD$

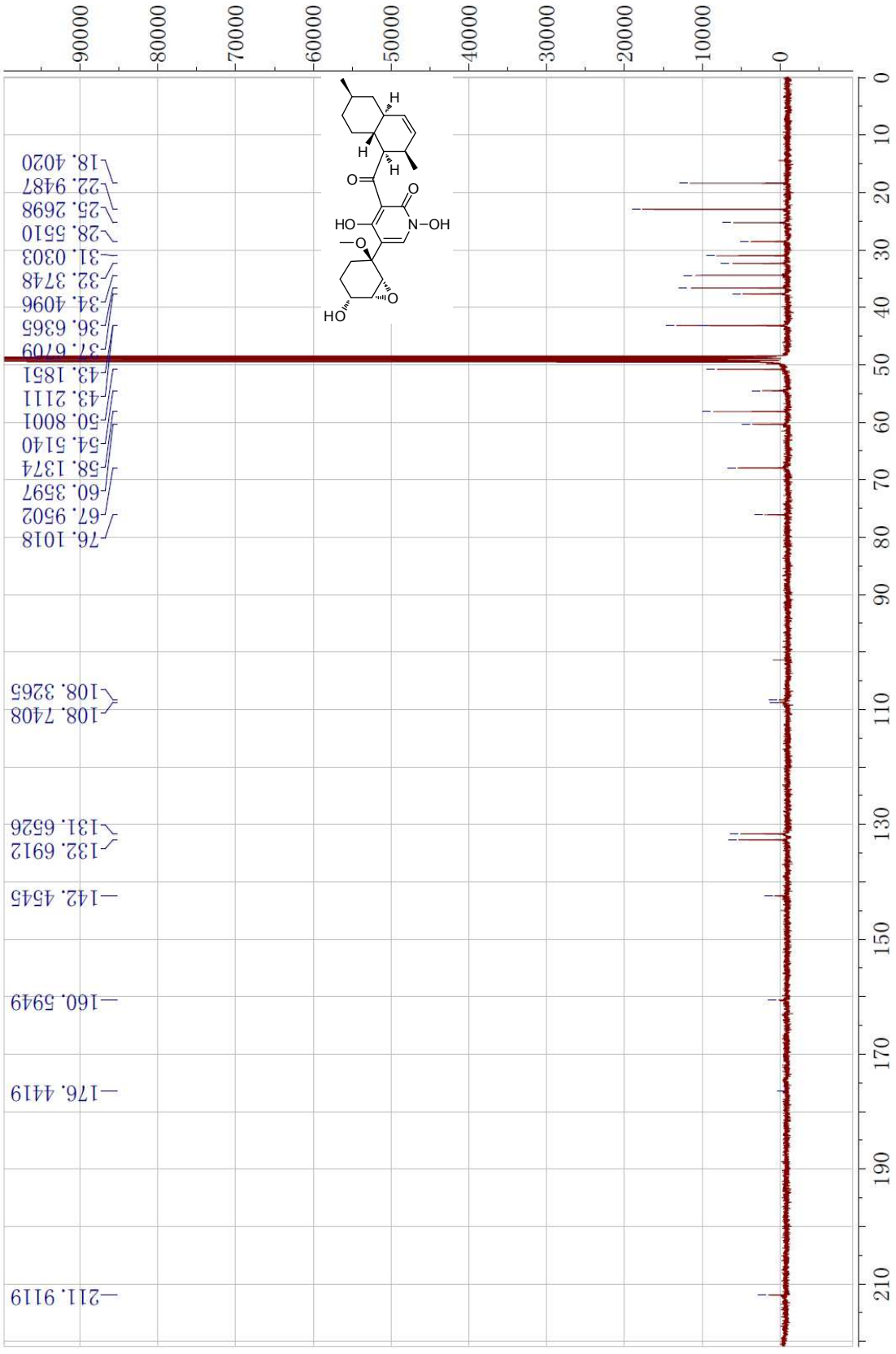

**Figure S24**. The HMQC spectrum of arthpyrone C (**3**) in $CD_3OD$

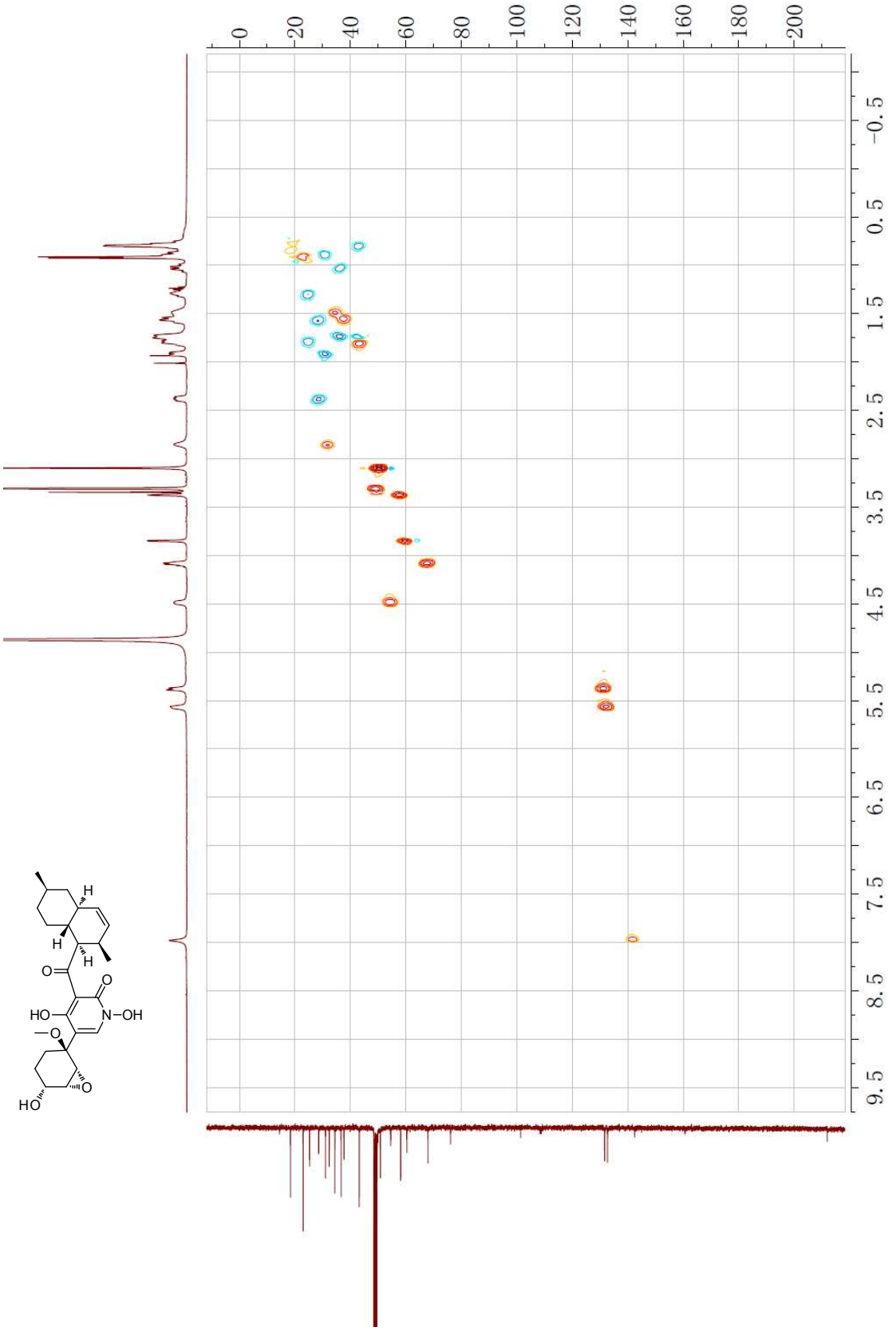

**Figure S25**. The $^{1}H$-$^{1}H$ COSY spectrum of arthpyrone C (**3**) in $CD_3OD$

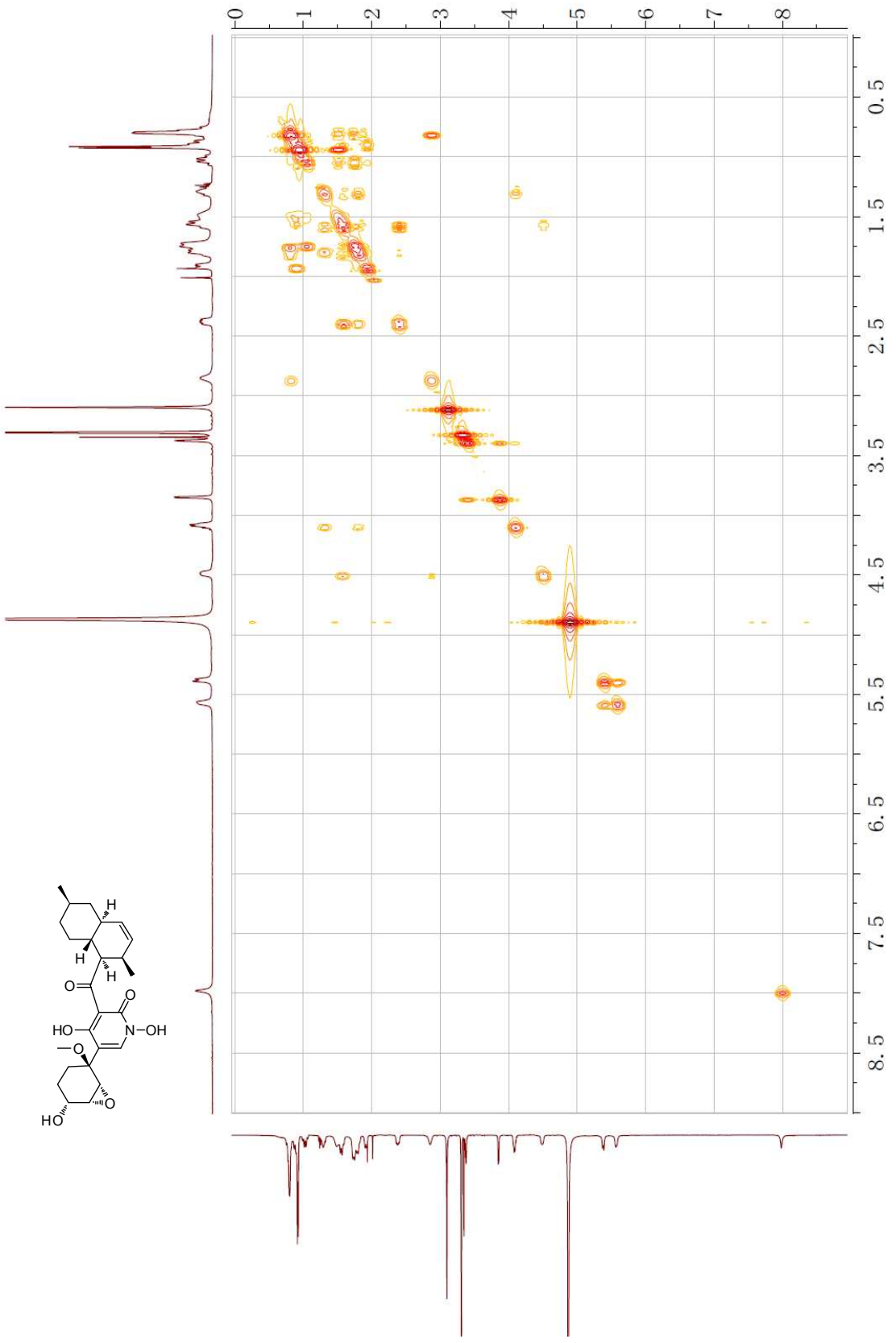

**Figure S26**. The HMBC spectrum of arthpyrone C (**3**) in $CD_3OD$

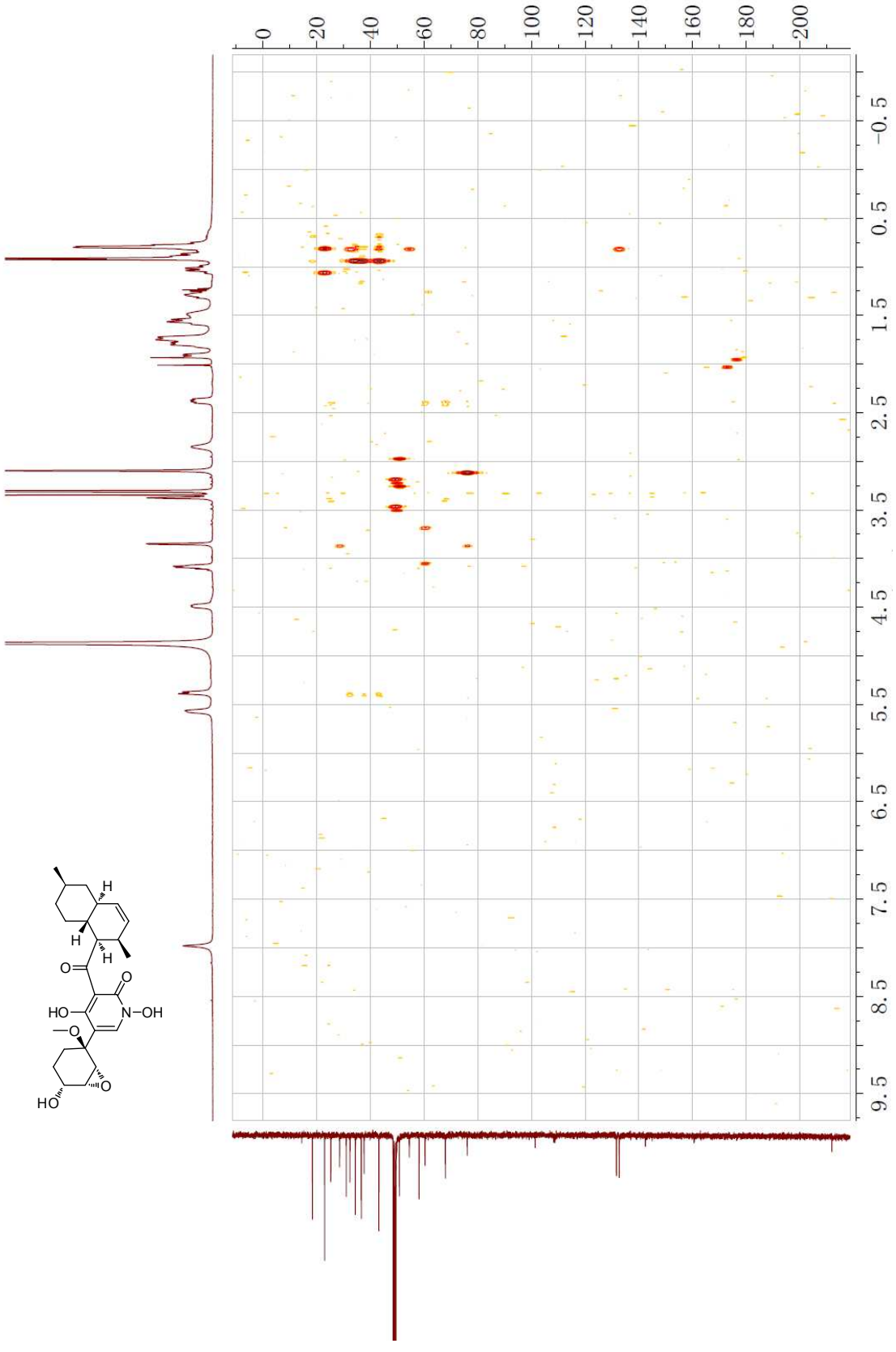

**Figure S27**. The NOESY spectrum of arthpyrone C (**3**) in $CD_3OD$

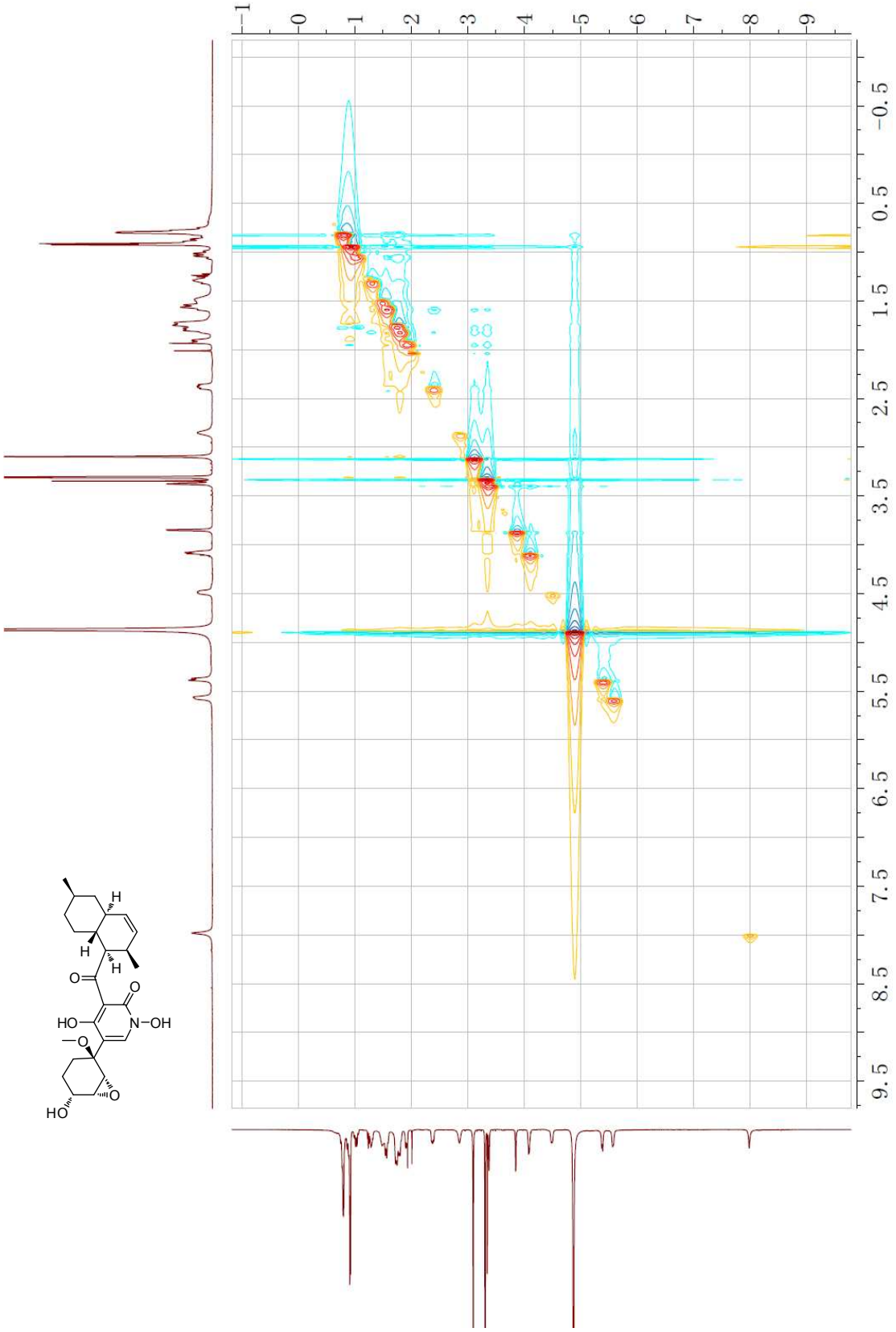

**Figure S28**. The HRESIMS spectrum of arthpyrone C (**3**)

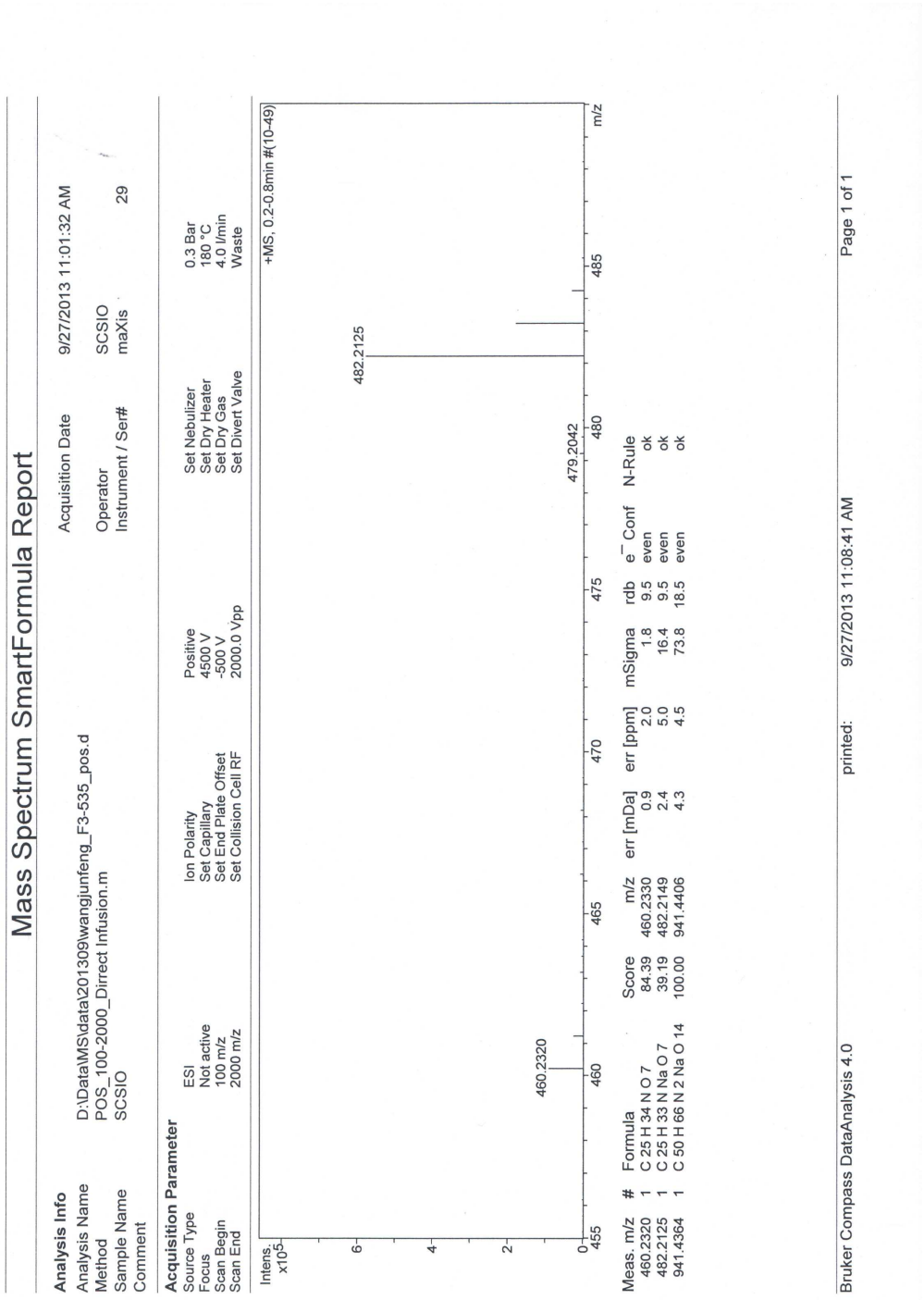

**Figure S29**. Analyzed compounds **1** and **2** by a chiralcel OD-H column